Reviewed Preprint
v1 • August 22, 2025
Not revised

Reviewed Preprint
v2 • May 29, 2026
Revised by authors

Dynamic assembly of malate dehydrogenase-citrate synthase multienzyme complex in the mitochondria

Joy Omini, Inga Krassovskaya, Taiwo Dele-Osibanjo, Connor Pedersen, Toshihiro Obata

Department of Biochemistry and Center for Plant Science Innovation, University of Nebraska-Lincoln, Lincoln, United States

For correspondence: tobata2@unl.edu

Competing interests: No competing interests declared

Funding: See page 31

Reviewing editor: P Darrell Neufer, Wake Forest University School of Medicine, United States

eLife Assessment

This **important** study provides novel information on multi-enzyme complexes, known as metabolons, that form between sequential enzymes in a metabolic pathway. Using an innovative NanoBiT split-luciferase system, the authors present **compelling** evidence that malate dehydrogenase (MDH1) and citrate synthase (CIT1) dynamically associate under different metabolic conditions in Saccharomyces cerevisiae. The findings suggest the dynamic MDH1-CIT1 interaction facilitates control of TCA pathway flux rate.

https://doi.org/10.7554/eLife.107953.2.sa4

Abstract

The tricarboxylic acid (TCA) cycle enzymes malate dehydrogenase (MDH1) and citrate synthase (CIT1) form a multienzyme complex, referred to as a metabolon, that channels intermediate oxaloacetate between their reaction centers. Given that the MDH1-CIT1 metabolon enhances pathway reactions in vitro, its dynamic assembly is hypothesized to contribute to TCA cycle regulation in response to cellular metabolic demands. Here, we demonstrated that yeast mitochondrial MDH1 and CIT1 dissociated when aerobic respiration was suppressed by the Crabtree effect and associated when the respiratory activity was enhanced by acetate.

Pharmacological TCA cycle inhibition dissociated the complex, whereas electron transport chain inhibition enhanced the interaction. The multienzyme complex assembly was related to the mitochondrial matrix acidification and oxidation, as well as cellular levels of malate, fumarate, and citrate. These factors significantly affected the MDH1-CIT1 complex affinity in vitro. Especially, variations in buffer pH within the physiological pH range between 6.0 and 7.0 in the mitochondrial matrix significantly impacted the MDH1-CIT1 affinity. These results demonstrate the dynamic association and dissociation of the MDH1-CIT1 metabolon and its relationship with respiratory activity, supporting metabolon dynamics as an integral factor in metabolic regulation governed by multiple factors such as mitochondrial pH and metabolite levels.

Introduction

Enzymes catalyzing sequential reactions can interact to form a multienzyme complex, often called a ‘metabolon,’ which channels the metabolic intermediate within the complex. Metabolite channeling can mediate pathway reactions by concentrating the reaction intermediates near the enzyme active site and sequestering them from competing reactions (Obata, 2020; Spivey and Ovádi, 1999; Wheeldon et al., 2016). Thus, the dynamic assembly of multienzyme complex is believed to quickly regulate cellular metabolic flux by changing their degree of association and dissociation without involving time-consuming and resource-demanding protein synthesis,

degradation, and modification (Halper and Srere, 1977; Morgunov and Srere, 1998; Obata, 2019; Omini et al., 2024; Srere, 1985; Sumegi et al., 1993). However, limited experimental evidence shows metabolon dynamics and the mechanisms regulating its association.

The tricarboxylic acid (TCA) cycle multienzyme complex composed of malate dehydrogenase (MDH) and citrate synthase (CS) is conserved in all organisms analyzed so far, including animals, bacteria, yeast, and plants (Meyer et al., 2011; Morgunov and Srere, 1998; Robinson et al., 1987; Zhang et al., 2017). MDH and CS catalyze the key steps in respiratory metabolism as their reactions comprise the carbon entry steps from the glycolytic processes as malate and acetyl-CoA, respectively (Sweetlove et al., 2010). MDH-CS complex is considered a dynamic protein complex (Bulutoglu et al., 2016; Omini et al., 2021) that protects the channeled intermediate, oxaloacetate, from degradation and competing pathways in the bulk phase of the cell (Bulutoglu et al., 2016).

Importantly, MDH-CS complex formation and oxaloacetate channeling are considered essential for the forward TCA cycle flux to occur since MDH forward reaction to synthesize oxaloacetate is thermodynamically unfavorable in physiological conditions (Fukuda et al., 2008). These findings suggest that the dynamic association and dissociation of the MDH-CS multienzyme complex play a role in coordinating the TCA cycle and associated metabolic pathways. To address this hypothesis, this study focuses on demonstrating the in vivo dynamics of the MDH-CS complex in relation to respiratory states, a crucial aspect of achieving metabolic regulation. Another key requirement, the direct impacts of the metabolon on pathway flux, will be addressed in a separate study.

This study utilized the yeast mitochondrial MDH (MDH1)-CS (CIT1) multienzyme complex as the model. Budding yeast, *Saccharomyces cerevisiae*, dramatically rearranges its central carbon metabolism in response to changes in nutrient availability and stress conditions (Causton et al., 2001; Rep et al., 1999; Rolland et al., 2002). Remarkably, yeast respiratory metabolism, involving aerobic respiration and fermentation, is highly adaptable to substrate availability (Pfeiffer and Morley, 2014). When oxygen and non-fermentable respiratory substrates, such as acetate, are abundant, aerobic respiration is upregulated, with increased carbon flux through the TCA cycle (Gerstmeir et al., 2003; Lee et al., 2011). In the presence of fermentable sugars, such as glucose and fructose, the fermentation pathway is upregulated, and aerobic respiration is repressed, even when oxygen is available (Zhang et al., 2022). Furthermore, aerobic respiration and fermentation cooperate in the presence of a poorly fermentable carbon source like raffinose (Guaragnella et al., 2013). Application of fermentable substrates to respiring yeast cells induces a substantial shift from aerobic respiration to fermentation, known as the 'Crabtree effect,' involving a massive transcriptional rearrangement of enzyme genes related to aerobic respiration and fermentation (Gancedo, 1998; Ronne, 1995; Thierie and Penninckx, 2010). This inducible metabolic shift in yeast makes it an ideal model for investigating the dynamic relationship between the MDH1-CIT1 multienzyme complex and TCA cycle flux. Understanding the mechanisms of the Crabtree effect is crucial for metabolic engineering applications to enhance the supply of TCA cycle intermediates for desired product synthesis (Yin et al., 2015) and for gaining insights into metabolic regulation in other eukaryotic systems, including cancer cells, which exhibit metabolic shifts similar to the Crabtree effect (Diaz-Ruiz et al., 2011).

Various allosteric regulators and environmental factors, including pH and redox state, affect MDH and CS enzyme activities (Beeckmans, 1984; Williamson and Cooper, 1980). These factors alter protein conformations, influencing the MDH-CS complex affinities. Previous in vitro studies have demonstrated that NAD^+, malate, succinate, acetyl-CoA, α-ketoglutarate, and acidic pH enhance the MDH-CS interaction, while NADH, citrate, and basic pH weaken it (Omini et al., 2024, 2021; Tompa et al., 1987; Wu and Minteer, 2015). These allosteric regulators promote the MDH-CS interaction when the TCA cycle substrates are abundant and products are limited, indicating the role of the MDH-CS multienzyme complex in the TCA cycle feedback regulation. The electron transport chain activity affects the mitochondrial matrix pH, redox state, and ATP content and is closely related to cellular respiratory flux distributions (Santo-Domingo and Demaurex, 2012)).

Therefore, the MDH-CS multienzyme complex may associate and dissociate according to the microenvironment in the mitochondrial matrix, such as metabolite concentrations, pH, redox state, and energy levels.

We adopted a NanoBiT protein-protein interaction assay system (Dixon et al., 2016) to monitor real-time multienzyme complex interactions in living yeast cells using continuous microplate readings. The NanoBiT split-luciferase system is based on the 18 kDa NanoLUC luciferase derived from deep-sea shrimp. The small size of this reporter is designed to minimize structural and behavioral interference with the target proteins, while offering a dynamic range and brightness approximately 150-fold greater than those of conventional luciferases, enabling detection of weak, transient interactions. The NanoBiT subunits exhibit low intrinsic affinity (K_D = 190 μM) and rapid association and dissociation kinetics (k_{on} = 500 $M^{-1}s^{-1}$, k_{off} = 0.2 s^{-1}), ensuring that the luminescent complex formation is dictated by the interaction of the fused proteins rather than the affinity of the tags themselves (Dixon et al., 2016). While other fluorescence-based methods, such as FLIM-FRET and BRET, are widely used for *in vivo* protein-protein interaction studies, they are limited in yeast microplate assays due to high cellular autofluorescence. The NanoBiT system overcomes these constraints, providing semi-quantitative monitoring of relative fluctuations in protein interaction levels over time across a diverse range of metabolic conditions.

In this study, the NanoBiT system examined the MDH1-CIT1 multienzyme complex association in the presence of various carbon sources and respiratory inhibitors. The results showed the relationship between respiratory activity and the dynamic MDH1-CIT1 complex assembly.

Analysis of the mitochondrial matrix microenvironment using fluorescent biosensors and cellular metabolite profiles revealed crosstalk among cellular respiratory status, the MDH1-CIT1 interaction, and the mitochondrial matrix microenvironment, including pH. These findings indicate the functional dynamics of the MDH-CS multienzyme complex and how they coordinate with the metabolic states of the TCA cycle and adjacent pathways.

Results

MDH1-CIT1 interaction was detected exclusively in respiratory conditions

We employed a NanoBiT split-luciferase system (Dixon et al., 2016) for semi-quantitative relative detection of the MDH1-CIT1 multienzyme complex association in living yeast cells. The codon-optimized sequences of nano-BIT subunits were integrated into the direct downstream of the MDH1 and CIT1 exons in the yeast genome by gene homologous recombination to fuse the NanoBiT subunits to the native enzymes. The NanoBiT subunits reconstitute the NanoLUC holoenzyme to produce luciferase signals when MDH1 and CIT1 are in proximity. The affinity between the NanoBiT subunits is very low and does not stabilize the interactions of the tagged proteins (Dixon et al., 2016). The integration of NanoBiT subunits had no significant effect on the cellular growth rate or cellular MDH and CS enzyme activities (Figure 1 – figure supplement 1). Although the MDH1-CIT1 reporter line did not show a detectable luciferase signal when it was grown in a fermentation condition (glucose-containing SD media; SD-Gluc), it showed a substantial luciferase signal in mixed-respiration (raffinose-containing SD media; SD-Raff) and respiration (acetate-containing SD media; SD-Acet) conditions (Figure 1A). These results indicate that MDH1 and CIT1 interact under respiratory conditions. The MDH1-CIT1 interaction can be related to the oxidative respiration and the TCA cycle activity since oxygen consumption was detected only in SD-Raff and SD-Acet media but not in the SD-Gluc medium (Figure 1B), as previously reported (Klein et al., 1998; Polakis and Bartley, 1965; Rep et al., 1999; Rolland et al., 2002; Strittmatter, 1957). However, MDH1 and CIT1 expressions were downregulated in SD-Gluc growing cells near the detection limit (Figure 1C), making it difficult to conclude if the undetectable MDH1-CIT1 interaction was due to complex dissociation or low protein levels.

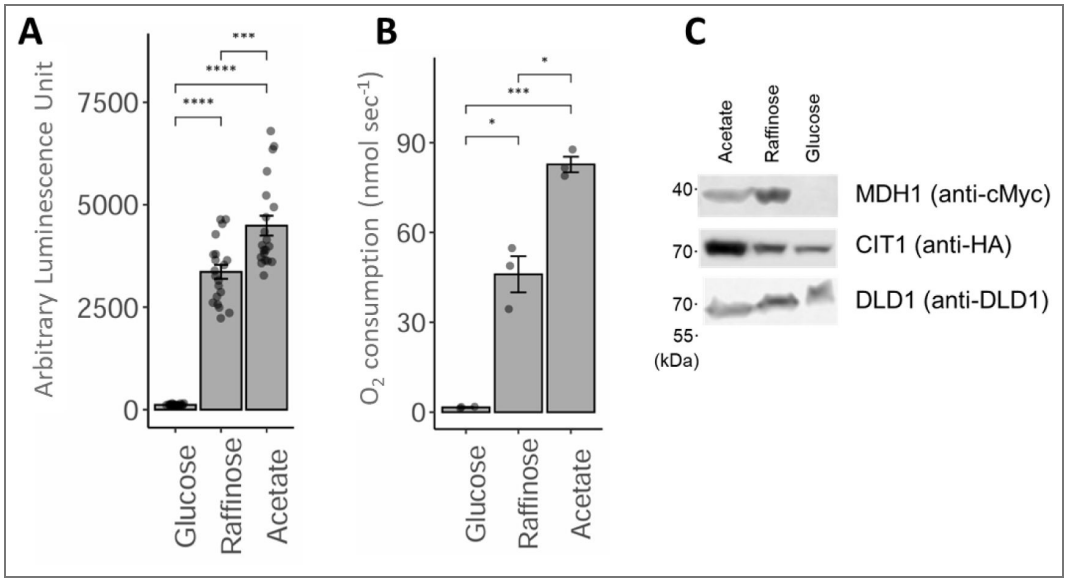

Figure 1. MDH1-CIT1 interaction under respiration, fermentation, and mixed-respiration conditions.

Yeast cells were grown in the minimum media containing acetate (SD-Acet), glucose (SD-Gluc), and raffinose (SD-Raff) to the exponential growth phase. **(A)** Luciferase signal indicating MDH1-CIT1 complex interaction (N=20). **(B)** Cellular oxygen consumption rate (N=3). **(C)** MDH1 and CIT1 protein levels detected by Western blotting. Numbers on the left indicate the position of the molecular weight markers. DLD1 is a loading control of mitochondrial protein. Full gel images are in Figure 1 – figure supplement 2. In A and B, data are presented as mean ± SEM. and the differences between conditions were tested by Student's *t*-test. Asterisks indicate significant differences (*, $p<0.05$; **, $p<0.01$; ***, $p<0.001$; ****, $p<0.0001$; ns, not significant).

Crabtree induction reduced the MDH1-CIT1 interaction

To test the relationship between respiratory activity and the MDH1-CIT1 complex association when MDH1 and CIT1 enzymes are abundant in the cell, we monitored the time course of the MDH1-CIT1 interaction after a rapid shift from aerobic to anaerobic respiration via the Crabtree effect. The Crabtree effect was induced by applying 2% glucose to the SD-Raff-grown MDH1-CIT1 NanoBiT reporter line (Figure 2, Figure 2 – figure supplement 1). The luciferase signals only slightly changed for 30 min upon glucose application, followed by a steep decline. In contrast, the control cells retained the initial signal level for 100 min (Figure 2A, Figure 2 – figure supplement 1D). Decrease in the MDH1-CIT1 interaction was validated by a co-immunoprecipitation assay at 1.5 and 2.5 hours after the glucose application (Figure 2 – figure supplement 1A). Other Crabtree inducers, such as fructose and sucrose, also reduced the MDH1-CIT1 interaction, while the addition of non-fermentable sugars, including galactose, caused no significant change in MDH1-CIT1 interaction (Figure 2 – figure supplement 2A-D, Figure 2 – figure supplement 3), likely due to raffinose in the media suppressing its effects. The signal decline following glucose application was partially reversed by co-application with a fermentation inhibitor, 100 mM phosphate (van Urk et al., 1989; Figure 2A). Phosphate co-application slowed the decrease of luciferase signal compared to the glucose-applied cells, and the signal was not statistically significantly lower than the control until 80 min after application. The oxygen consumption rate significantly decreased when glucose was added to SD-Raff-grown cells but was slightly recovered by co-application of glucose with phosphate (Figure 2 – figure supplement 2E). These results indicate that the respiratory suppression by the Crabtree effect is related to MDH1-CIT1 complex disruption.

MDH1 protein level monitored with the yeast strain expressing MDH1 fused with full-length NanoLUC luciferase showed a 20% decline within 100 min upon glucose addition (Figure 2, Figure 2 – figure supplement 1B). Western blotting also showed a slight decrease in the MDH1 and CIT1 levels (Figure 2 – figure supplement 1C). The time course of the MDH1-CIT1 NanoBiT signal was inconsistent with that of MDH1-NanoLUC, and the 20% decline in protein content cannot fully explain the decrease of MDH1-CIT1 signal by over 50% within 100 min after glucose addition (Figure 2A, Figure 2 – figure supplement 1B). The reduction of MDH1-CIT1 interaction was not accompanied by the MDH1 and CIT1 abundance in a repeated experiment (Figure 2 – figure supplement 1D-E). The interaction index, calculated by normalizing the NanoBiT signal to MDH1 and CIT1 abundances measured with MDH1-NanoLUC and CIT1-NanoLUC (see Materials and Methods), showed reduced interaction after 60 min of glucose application.

Therefore, the decline in the MDH1-CIT1 NanoBiT signal reflects the MDH1-CIT1 complex dissociation co-occurring with the Crabtree effect, even though we cannot exclude a partial effect of protein degradation (Litsios et al., 2018).

Oxidative respiration significantly influences the microenvironments in the mitochondrial matrix (Beeckmans, 1984; Williamson and Cooper, 1980). To assess if the MDH1-CIT1 interaction decline is related to the changes in the microenvironments of the mitochondrial matrix by the Crabtree effect, we monitored the mitochondrial matrix pH, ATP concentration, and redox state by expressing fluorescent biomarkers, pHluorin, mito-GoAteam2, and mito-roGFP1, respectively, in the mitochondrial matrix of the MDH1-CIT1 reporter line (Figure 2 – figure supplement 4A-D).

Mitochondrial matrix pH in the SD-Raff-grown cells was 7.2 and temporally declined to 6.8 in the first 25 min of glucose application. The control cell matrix pH gradually decreased to 6.2 and remained lower than in glucose-applied cells (Figure 2B). The alterations of the MDH1-CIT1 interaction and mitochondrial matrix parameters in the control condition are not due to carbon starvation, since 2% raffinose application had no significant effect (Figure 2 – figure supplement 4E). The redox state stayed around -288.0 mV in both the control and glucose cells (Figure 2C). The ATP level slightly increased during the experimental period of 100 min in both the control and glucose cells, with slightly but significantly lower levels in the glucose than in the control cells from 55 min to 100 min (Figure 2D). Thus, mitochondrial matrix pH and ATP levels were

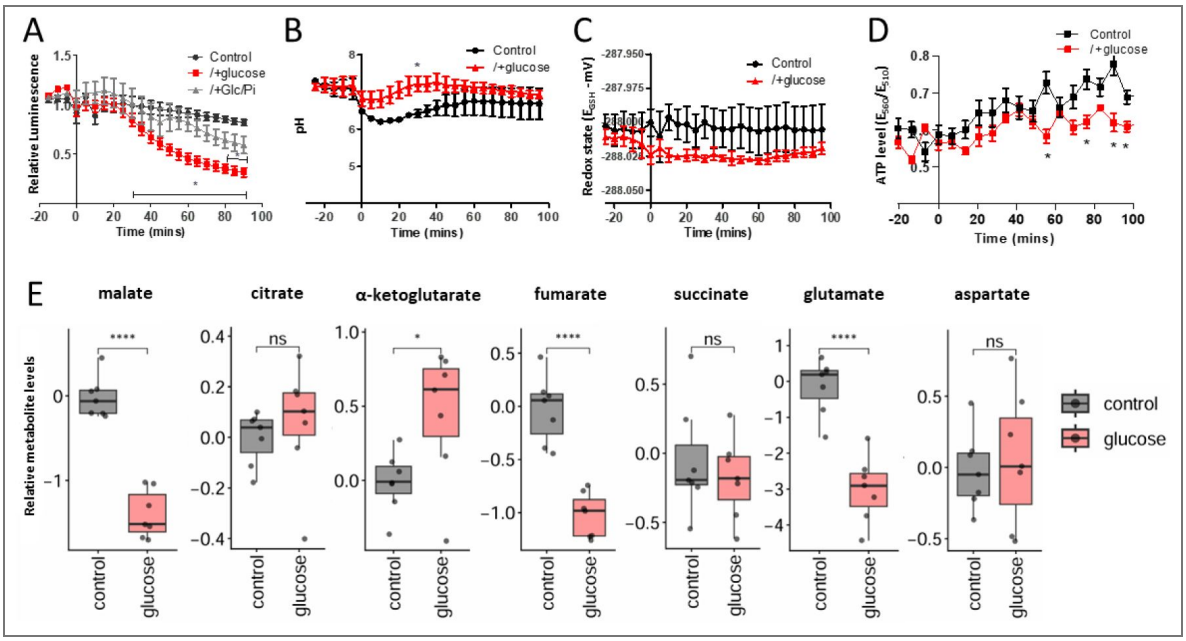

Figure 2. MDH1-CIT1 complex association, mitochondrial microenvironments, and cellular metabolite levels during Crabtree effect induction.

Cells were cultured in fresh SD-Raff media in the control condition (black). The Crabtree effect was induced by the 2% glucose application to the SD-Raff-grown cells at 0 min (red). **(A)** NanoBIT signal indicating MDH1-CIT1 interaction. Relative luciferase unit (RLU) was calculated by normalizing the luciferase signals tothe average signals during three pre-treatment time points. SD-Raff-grown cells were also co-treated with 2% glucose and a fermentation inhibitor, 100 mM phosphate, at 0 min (gray). **(B)** Mitochondrial matrix pH. **(C)** Mitochondrial matrix redox states as GSH/GSSG equivalent (mV). **(D)** Mitochondrial matrix ATP level indicated by the ratio between 560 and 510 nm emission signals. All data in A-D are presented as mean ± s.d. (N=4). **(E)** Cellular metabolite levels at 80 min. The boxes, lines, error bars, and points indicate interquartile range, median, minimum, and maximum values, and outliers, respectively (N=7). Statistical differences against the control samples were assessed using the Student's *t*-test at each time point. Asterisks indicate significant differences (*, $p<0.05$; **, $p<0.01$; ***, $p<0.001$; ****, $p<0.0001$; ns, not significant).

maintained after glucose was applied to cells, while they decreased and increased in control cells during the experimental period, indicating that mitochondrial pH and ATP levels are associated with MDH-CS complex dissociation during the Crabtree induction.

Our previous in vitro study showed that metabolite abundance influences the MDH-CS complex interaction (Omini et al., 2021). To assess the possible roles of metabolite accumulation in controlling MDH1-CIT1 complex interaction, we determined the cellular levels of 38 metabolites (Data S1) by gas chromatography-mass spectrometry (GC-MS). We focus here on the intermediates of the TCA cycle and related pathways (Figure 2E). At 80 min after 2% glucose application to SD-Raff-grown cells, malate, citrate, fumarate, and glutamate levels decreased, while α-ketoglutarate content increased significantly compared to the control cells (Figure 2G). Thus, the glucose-induced shift from aerobic respiration to fermentation altered the intracellular metabolite profile in SD-Raff-grown cells, potentially influencing the MDH1-CIT1 affinity.

MDH1-CIT1 complex interacts in relation to the TCA cycle activity

We further assessed the relationship between the MDH1-CIT1 complex association and TCA cycle activity. Acetate supplies acetyl-CoA to the TCA cycle and enhances its activity (Cavero et al., 2003). The application of 1% sodium acetate gradually increased the MDH1-CIT1 interaction while MDH1 and CIT1 protein abundance slightly reduced (Figure 3A, Figure 3 – figure supplement 1 A-D). The TCA cycle activation by ethanol (Schüller, 2003) also enhanced the complex association (Figure 3 – figure supplement 1E). However, it is accompanied by an increase in MDH1 and CIT1 abundance (Figure 3 – figure supplement 1F&G), making the effects of ethanol on the complex association unclear (Figure 3 – figure supplement 1H). On the other hand, TCA cycle inhibition by 5 mM sodium arsenite, which impedes α-ketoglutarate dehydrogenase (Lee et al., 2011), led to a decline in MDH1-CIT1 interaction within 10 min (Figure 3B, Figure 3 – figure supplement 1 I-L). Aminooxyacetate (AOA) is an aminotransferase inhibitor and reduces TCA cycle activity by blocking the malate-aspartate NADH shuttle, which intersects with the cycle (Borst, 2020; Eto et al., 1999; Molinié et al., 2022). The MDH1-CIT1 interaction gradually reduced following 0.5 mM AOA application (Figure 3C, Figure 3 – figure supplement 1M-P). These results support that the MDH1-CIT1 multienzyme complex association is related to TCA cycle activity.

Mitochondrial matrix pH declined to 6.1 immediately after acetate application (Figure 3D). Mitochondrial pH went slightly lower than that of the control cells after 40 min of TCA cycle inhibition by arsenite (Figure 3E), while AOA application had no effect on mitochondrial pH (Figure 3F). The mitochondrial matrix redox state was gradually increased in the control cells during the experimental period, while it was kept constant in the cells treated by acetate, arsenite, and AOA (Figure 3G-I), resulting in the significantly lower mitochondrial matrix redox state in the treated cells in the latter half of the experimental period. Mitochondrial ATP level was decreased by acetate treatment after 40 min (Figure 3J), although arsenite and AOA showed no effect on the mitochondrial ATP levels within the experimental period (Figure 3J&K). These changes in mitochondrial microenvironments did not show clear, direct relationships with the MDH1-CIT1 interaction.

We evaluated the cellular metabolite profile after treatment of SD-Raff grown cells for 80 min with 1% acetate, 5mM arsenite, and 0.5 mM AOA to determine the relationship between change in metabolite levels and the MDH1-CIT1 complex interaction (Figure 3M). Acetate application significantly reduced malate, α-ketoglutarate, fumarate, succinate, and glutamate levels, while aspartate abundance significantly increased. Inhibition of the TCA cycle by arsenite significantly reduced the levels of all TCA cycle metabolites other than α-ketoglutarate. Aspartate and glutamate were also decreased, and glutamate was almost depleted in the cell (Figure 3M). AOA significantly decreased citrate, fumarate, and succinate levels while it increased α-ketoglutarate abundance (Figure 3M). Reduction of TCA cycle organic acids by the TCA cycle inhibition may be related to the reduction in the MDH1-CIT1 interaction.

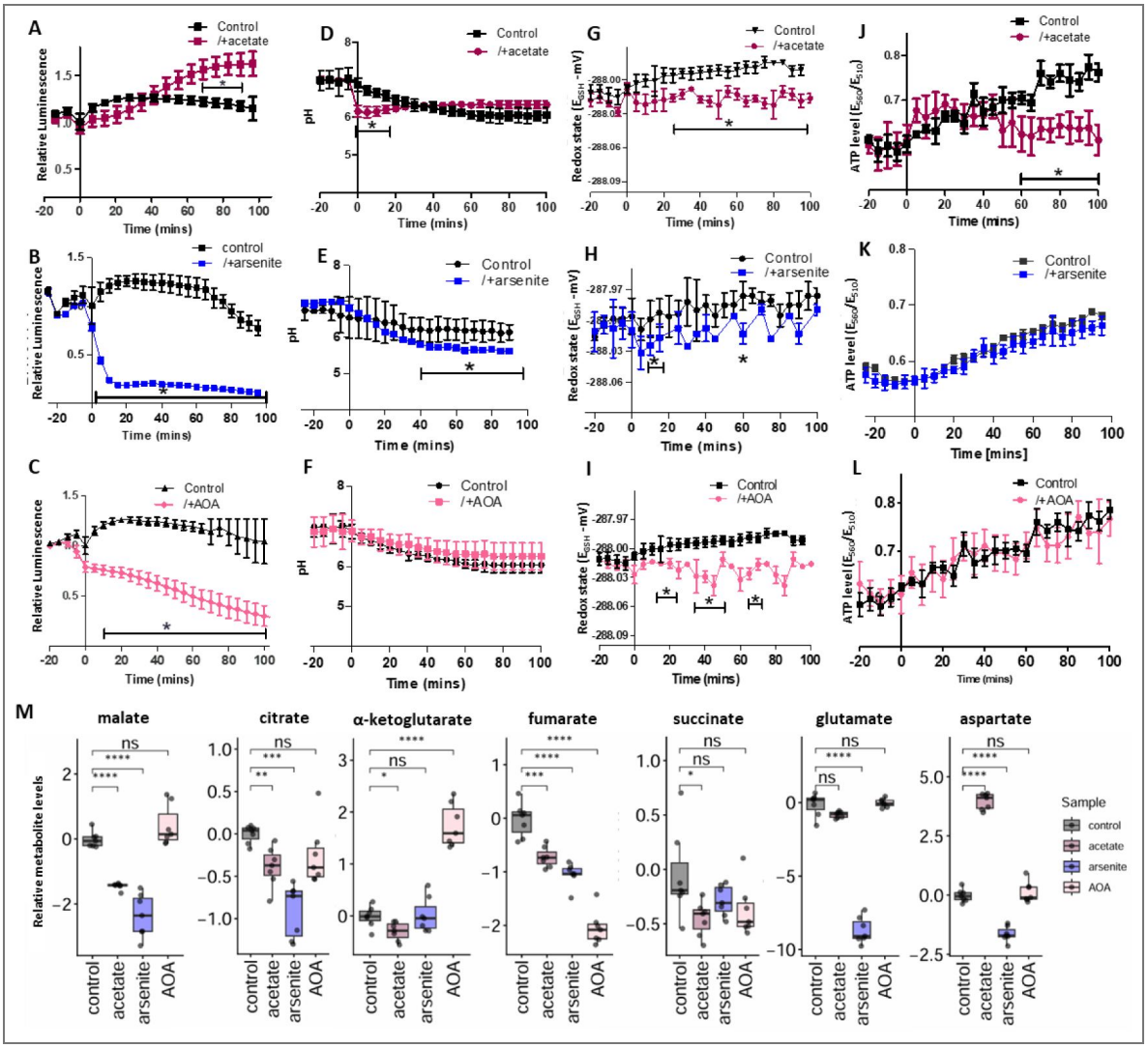

Figure 3. MDH1-CIT1 complex association, mitochondrial matrix microenvironments, and cellular metabolite levels following TCA cycle activation and inhibition.

Cells were cultured in SD-Raff media in the control condition (black). The TCA cycle activator (acetate, dark red) and inhibitors (arsenite, blue, and aminooxyacetate (AOA), pink) were applied at 0 min. **(A-C)** NanoBiT signal indicating MDH1-CIT1 interaction. Relative luciferase unit (RLU) was calculated by normalizing the luciferase signals by the average signals during three pre-treatment time points. **(D-F)** Mitochondrial matrix pH in control cells (black) and cells treated with acetate (dark red), arsenite (blue) and AOA (pink). **(G-I)** Mitochondrial matrix redox states as GSH/GSSG equivalent (mV). **(D, H, L)** Mitochondrial matrix ATP level indicated by the ratio between 560 and 510 nm emission signals of mito-GoATeam2 sensor. All data in A-L are presented as mean ± s.d. (N=4). **(M)** Cellular metabolite levels after 80 min of treatment. The boxes, lines, error bars, and points indicate interquartile range, median, minimum, and maximum values, and outliers, respectively (N=7). Statistical differences against the control samples were assessed using the Student's *t*-test at each time point. Asterisks indicate significant differences (*, $p<0.05$; **, $p<0.01$; ***, $p<0.001$; ****, $p<0.0001$; ns, not significant).

Electron transport chain inhibition enhanced the MDH1-CIT1 interaction, coinciding with matrix acidification

Mitochondrial electron transport chain (ETC) activity is directly related to the mitochondrial microenvironments (Selivanov et al., 2008). To further assess the effects of mitochondrial matrix microenvironments on MDH1-CIT1 complex interaction, we treated SD-Raff-grown cells with ETC inhibitors. Inhibition of ETC complex II, III, IV, and V with 20 mM malonate, 10 μM antimycin, 0.5 mM cyanide, and 1 mM oligomycin, respectively, significantly reduced oxygen consumption of SD-Raff-grown cells (Figure 4 – figure supplement 1), showing their effects on respiration. MDH1-CIT1 interaction was enhanced by ETC inhibitors with minor alterations of MDH1 and CIT1 protein levels (Figure 4A-C, Figure 4 – figure supplement 2), whereas the complex V (ATP synthase) inhibitor exerted no effect on MDH1-CIT1 interaction and mitochondrial matrix microenvironment in this experimental condition (Figure 4 – figure supplement 3A-D). Complex II inhibition slightly and temporally enhanced the MDH1-CIT1 interaction, although the increase was not statistically significant compared to the control (Figure 4A, Figure 4 – figure supplement 1B-E). The MDH1-CIT1 interaction was enhanced in the first 20 min of complex IV inhibition and reduced to the basal level afterward (Figure 4B, Figure 4 – figure supplement 2E-H). Complex III inhibition by antimycin slowly increased MDH1-CIT1 interaction, and the signal increase peaked at 60 min of treatment (Figure 4C; Figure 4 – figure supplement 2I-L).

Mitochondrial matrix pH was reduced by all ETC inhibitor treatments (Figure 4D-F), although the effect was very small in malonate-treated cells (Figure 4D). The matrix pH was transiently decreased and exhibited an inverse relationship with the MDH1-CIT1 interaction (Figure 4E). The mitochondrial matrix pH was reduced to 5.5 immediately after antimycin application and remained at the same level for 100 min (Figure 4F). These treatments show minor effects on the redox state of the mitochondrial matrix (Figure 4 G-I). The matrix was gradually oxidized following antimycin treatment, but the difference relative to control cells was not statistically significant (Figure 4I). ETC inhibitions also showed relatively minor effects on mitochondrial ATP levels (Figure 4J-L), except for the reduction of ATP levels at the first 20 min of Complex IV inhibition (Figure 4K), which is accompanied by the increase of MDH1-CIT1 interaction (Figure 4B). These results indicate the relationship between MDH1-CIT1 interaction and mitochondrial matrix acidification.

Since the results indicate a relationship between mitochondrial matrix pH and the MDH1-CIT1 interaction, we have tested the effect of an uncoupler, carbonyl cyanide 3-chlorophenylhydrazone (CCCP), on this interaction (Figure 4 – figure supplement 4), which is expected to equilibrate the mitochondrial pH with the medium pH of 5.8 (Rosado et al., 2008). Treatment with 2 μM CCCP increased the MDH1-CIT1 interaction signal, suggesting that acidic pH enhances complex association (Figure 4 – figure supplement 4A&D). However, this result should be interpreted with caution, as CCCP treatment compromised the luciferase signal from MDH1 and CIT1 fused to full-length NanoLUC (Figure 4 – figure supplement 4B&C).

Cellular metabolite profiles were determined 30 min after malonate and cyanide treatments and 80 min after antimycin and oligomycin treatments. Complex II and V inhibition did not significantly alter cellular metabolite levels other than the malate and aspartate accumulation in malonate-treated cells (Figure 4M, Figure 4 – figure supplement 3E). Complex IV inhibition by cyanide significantly reduced citrate and glutamate levels, while malate, alpha-ketoglutarate, fumarate, and succinate levels significantly increased (Figure 4M). Complex III inhibition significantly decreased citrate and α-ketoglutarate levels and increased the malate level (Figure 4M). These results support the relationship between the levels of TCA cycle intermediates and MDH1-CIT1 interaction.

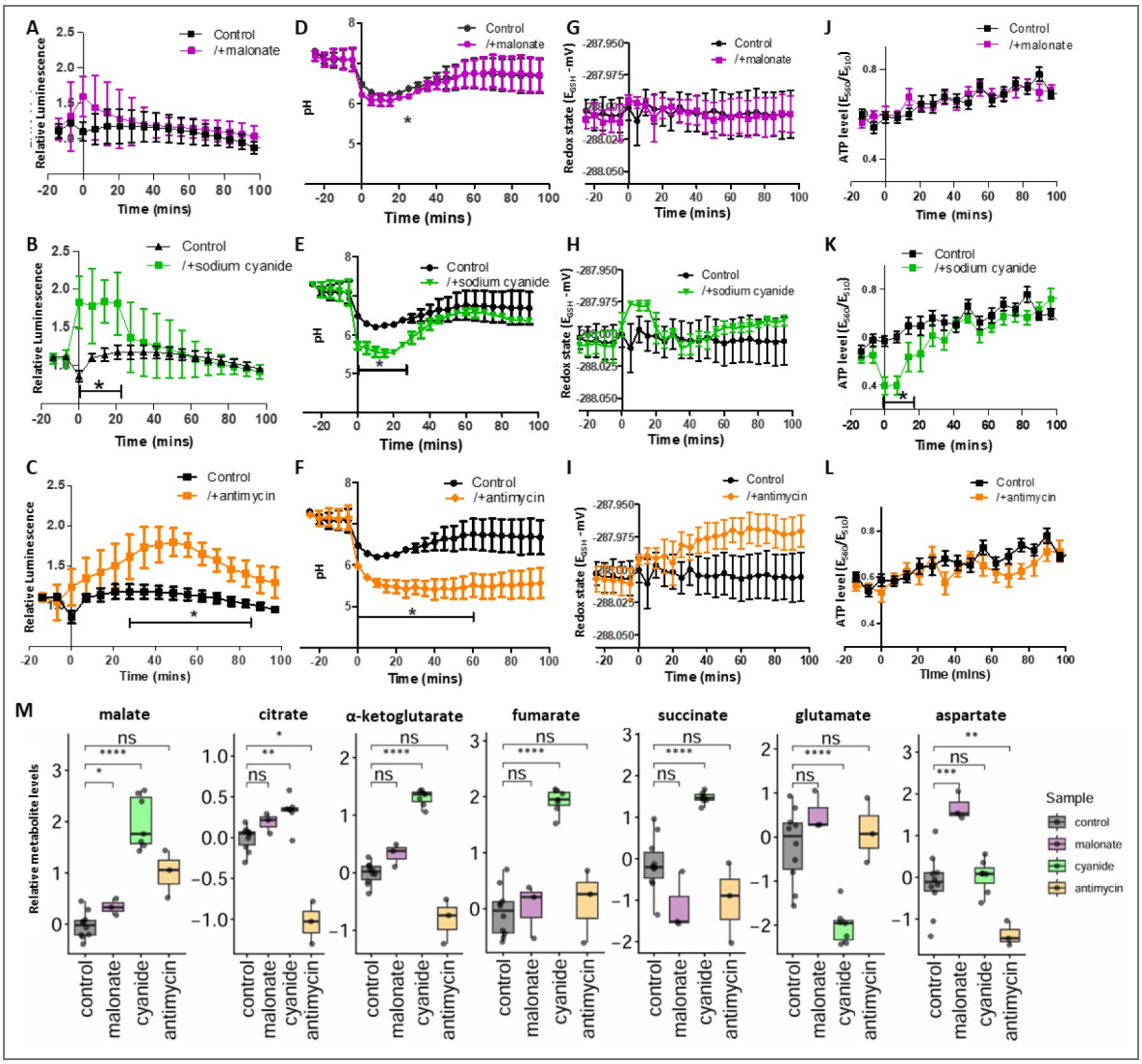

Figure 4. MDH1-CIT1 complex association, mitochondria microenvironments, and cellular metabolite levels following mitochondrial electron transport chain (ETC) inhibition.

Cells were cultured in SD-Raff media in the control condition (black). The ETC inhibitors for complex II (malonate, purple, **A-D**), complex IV (cyanide, green, **E-H**), and complex III (antimycin, orange, **I-L**) were applied at 0 min. **(A, E, I)** NanoBiT signal indicating MDH1-CIT1 interaction. Relative luciferase unit (RLU) was calculated by normalizing the luciferase signals by the average signals during three pre-treatment time points. **(B, F, J)** Mitochondrial matrix pH. **(C, G, K)** Mitochondrial matrix redox states as GSH/GSSG equivalent (mV). **(D, H, L)** Mitochondrial matrix ATP level indicated by the ratio between 560 and 510 nm emission signals of mito-GoATeam2 sensor. All data in A-L are presented as mean ± s.d. **(M)** Cellular metabolite levels after 30 min for malonate and cyanide and after 80 min for antimycin treatment. The boxes, lines, error bars, and points indicate interquartile range, median, minimum, and maximum values, and outliers, respectively. Statistical differences against the control samples were assessed using the Student's *t*-test at each time point. Asterisks indicate significant differences with $p<0.05$.

MDH1-CIT1 interaction is affected by pH, ATP concentration, and metabolite availability in vitro

To evaluate the specific effects of microenvironments and metabolite availability on the MDH1-CIT1 interaction, we investigated the MDH1-CIT1 affinity in vitro using recombinant proteins.

Acidic pH significantly enhanced the binding affinity of the MDH1-CIT1 complex (Figure 5A) within the physiological range observed in this study (Figure 2B, Figure 3D, Figure 4D, E, F). The K_d of the MDH1-CIT1 interaction was 3.48 μM at pH 7.2, while it was one magnitude lower at acidic pH (0.223 μM at pH 6.4 and 0.033 μM at pH 6.0). We also assessed the effects of the metabolites on the MDH1-CIT1 interaction (Figure 5B, Figure 5 – figure supplement 1). We tested malate, fumarate, citrate, α-ketoglutarate, succinate, glutamate, and aspartate since their cellular levels changed when the MDH1-CIT1 interaction altered (Figure 2E, Figure 3M, Figure 4M). Citrate destroyed the MDH1-CIT1 interaction, while malate and fumarate significantly enhanced complex affinity (Figure 5B). α-ketoglutarate, succinate, and aspartate slightly enhanced MDH1-CIT1 complex affinity, although glutamate did not affect the interaction (Figure 5 – figure supplement 1A). ATP also enhanced the MDH1-CIT1 complex affinity (Figure 5 – figure supplement 1B) as observed in porcine enzymes (Omini et al., 2021). Thus, malate, fumarate, citrate, ATP levels, and pH potentially influence the MDH1-CIT1 interaction in yeast mitochondria.

Discussion

Here, we report the relationships between respiratory activity and mitochondrial MDH1-CIT1 multienzyme complex interaction in living yeast cells. MDH1-CIT1 multienzyme complex dynamically associated and dissociated in response to respiratory status. This study is the first in vivo evidence in any organism showing the dynamic association and dissociation of the TCA cycle metabolon in real time. The MDH-CS metabolon, specifically, is considered essential for the forward TCA cycle flux due to its ability to overcome the unfavorable thermodynamics of MDH reaction under physiological oxaloacetate concentrations (Beeckmans and Kanarek, 1981; Huang et al., 2018). The results of this study demonstrate that the MDH1-CIT1 multienzyme complex associates when the TCA cycle is active and dissociates when it is suppressed, supporting the idea that metabolon dynamics are related to pathway regulation. Given that the MDH-CS metabolon is proposed to enhance pathway reactions (Bulutoglu et al., 2016; Fukuda et al., 2008), its dynamic assembly and disassembly would influence pathway activity. Together, these observations align with the proposed theory that metabolon dynamics act as a regulatory mechanism of metabolic flux (Noor et al., 2014; Obata, 2020).

The MDH1-CIT1 complex dissociated under conditions suppressing the TCA cycle. TCA cycle inhibition by arsenite and AOA induced dissociation of the MDH1-CIT1 complex (Figure 3B &C). In a physiological condition, the MDH1-CIT1 complex dissociated when Crabtree-inducing fermentable sugars were supplied to the media (Figures 1, 2, and Figure 2 – figure supplement 1-3). The Crabtree effect redistributes respiratory flux to stimulate fermentation and repress aerobic respiratory pathways, including the TCA cycle (Gancedo, 1998; Ronne, 1995). The metabolic shift by the Crabtree effect is a concerted action of multiple mechanisms, such as the suppression of enzyme gene expressions and the inhibition of mitochondrial transporters (Ahmadzadeh et al., 1996). Interestingly, glucose-induced rapid repression of mitochondrial respiration occurs at a rate that is too great to be explained only by the inhibition of enzyme synthesis, and additional forms of regulation are anticipated to be involved (Ahmadzadeh et al., 1996). The dissociation of the TCA cycle metabolon coincided with this repression (Figure 2A), highlighting metabolon dynamics as a potential additional mechanism to swiftly downregulate mitochondrial respiration during the Crabtree effect.

On the other hand, the MDH1-CIT1 complex interaction was enhanced under conditions that activate the TCA cycle. An increase in TCA cycle activity by the addition of acetate (Orlandi et al., 2014; Vilela-Moura et al., 2011) enhanced the MDH1-CIT1 complex interaction (Figure 3A), suggesting the role of the MDH-CS metabolon in facilitating TCA cycle activity.

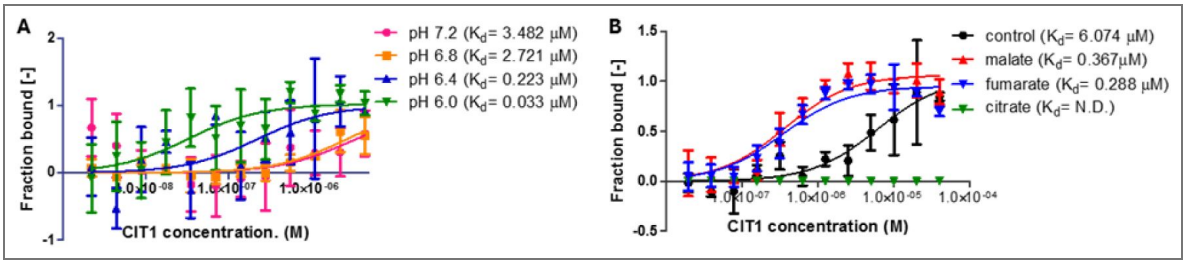

Figure 5. Effects of pH and metabolites on the yeast MDH1-CIT1 multienzyme complex affinity.

The affinity of the MDH-CS multienzyme complex was analyzed by microscale thermophoresis (MST) using fluorescently labeled MDH1 as the target and CIT1 as the ligand. Curves represent the response (fraction bound) against CIT1 concentration. Data is presented as mean ± s.d. (N=3). **(A)** Effects of pH. The MDH1-CIT1 interaction was determined in the buffer with pH 7.2 (pink), 6.8 (orange), 6.4 (olive green), 6.0 (green), and 5.8 (blue). **(B)** Effects of 10 mM malate (red), α-ketoglutarate (green), succinate (brown), citrate (blue), aspartate (purple), glutamate (pink), and fumarate (orange). The K_d values of MDH1-CIT1 interaction were shown next to the legend.

However, ETC inhibitions also increased MDH1-CIT1 interaction (Figure 4A-C), despite their inhibitory effects on oxidative respiration (Figure 4 - figure supplement 1) and the TCA cycle. This apparent contradiction can be explained by the transient nature of the response. The rise in MDH1–CIT1 interaction following ETC inhibition was transient, suggesting that it does not represent steady-state changes in respiratory activity. Instead, it is more likely linked to acute changes in the mitochondrial matrix microenvironment. Notably, the timing of the increased interaction coincided with changes in matrix pH, supporting a role for pH-dependent regulation (see below). These findings align with our model, which posits that the MDH1–CIT1 interaction is controlled by microenvironmental changes accompanying shifts in respiration. In the case of ETC inhibition, transient perturbations of the matrix microenvironment appear to be disconnected from steady-state respiratory output, thereby promoting MDH1–CIT1 interaction despite overall inhibition of respiration.

We also investigated the molecular mechanisms regulating MDH1-CIT1 complex dynamics. We previously reported that protein conformation changes induced by the solution pH and allosteric regulators affect porcine MDH-CS complex interaction in vitro (Omini et al., 2021). The recombinant yeast MDH1 and CIT1 showed similar responses to the porcine enzymes; MDH1-CIT1 affinity was higher in low pH and in the presence of upstream TCA cycle intermediates (malate and fumarate) but disrupted in the presence of reaction product (citrate; Figure 5). These factors can affect the TCA cycle metabolon formation in vivo. The relationship between these factors and the MDH1-CIT1 interaction observed in this study is summarized in Figure 6A.

We observed an enhanced MDH1-CIT1 interaction under conditions that lower mitochondrial matrix pH in vivo. The mitochondrial matrix pH decreased after adding acetate, corresponding to the enhanced MDH1-CIT1 interaction (Figure 3 A, D). The time courses of the temporal increase in MDH1-CIT1 interaction and pH decrease were inversely related following the complex III and IV inhibitions (Figure 4B, C, E, F; Figure 6A). The decrease in the pH from 7.5 to 6.0 ranges is remarkable since the K_d of MDH1-CIT1 association decreases by an order of magnitude within this pH range (Figure 5A). The mitochondrial matrix acidification under respiratory conditions likely favors the MDH1-CIT1 interaction. On the other hand, the mitochondria matrix pH was maintained around 7.2 in the presence of glucose (Figure 2D), which likely weakens the MDH1-CIT1 complex interaction. These results indicate that mitochondrial matrix pH, which is related to proton transport activity by the ETC, can stabilize or destabilize the MDH1-CIT1 complex, thereby regulating the MDH1-CIT1 interaction in response to respiratory activity (Figure 6B). Enhancing the MDH1-CIT1 interaction with the uncoupler CCCP (Figure 4 – figure supplement) also supports the prominent effect of pH.

Nevertheless, mitochondrial pH may influence the MDH1-CIT1 association, but it is not always the predominant factor regulating the interaction. The observed changes in pH and interaction do not consistently occur simultaneously following the Crabtree induction and acetate supplementation (Figs 2 & 3). TCA cycle inhibitions reduce the MDH1-CIT1 interaction without significantly affecting mitochondrial matrix pH (Figure 3B, C, E, F). These findings suggest that mitochondrial matrix pH can be a contributing factor, either favoring or disfavoring the interaction, rather than the primary regulator, which appears to be the direct induction and dissociation of the MDH1-CIT1 complex.

Little evidence in this study supports a primary role for mitochondrial matrix redox state or ATP levels in controlling MDH1–CIT1 interaction. Our in vitro analyses demonstrate that NAD(H) and ATP can modulate MDH1–CIT1 interaction (Figure 5 - figure supplement 1B; Omini et al., 2021), suggesting that these factors may contribute to complex dynamics. Although the lower matrix ATP level following glucose supplementation (Figure 2D) and matrix reduction upon arsenite and AOA-induced TCA cycle inhibition (Figure 3H&I) associated with decreased interaction (Figure 2A and 3B&C), these relationships were not consistently observed across conditions (Figure 6A), indicating that neither redox state nor ATP levels predict complex association in vivo. However, we cannot rule out their contribution under specific metabolic contexts not captured in the current study.

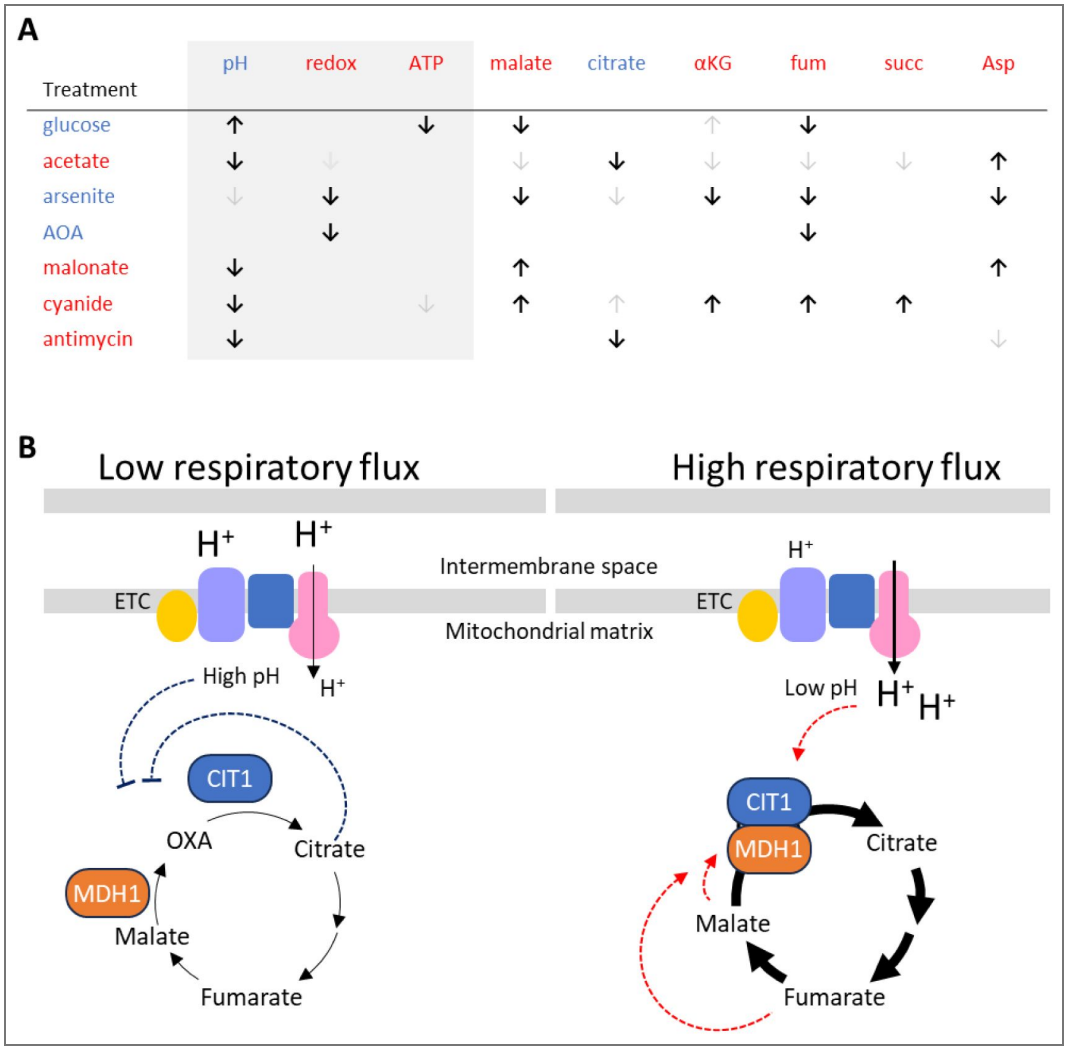

Figure 6. Relationship between the respiratory metabolism and the MDH1-CIT1 metabolon association.

(A) Summary of the effects of metabolic treatments on MDH1-CIT1 complex association, mitochondrial matrix parameters (pH, redox state, and ATP levels), and cellular metabolite levels. Each row corresponds to a specific metabolic perturbation. Blue and red labels indicate treatments that decrease or increase the complex association, respectively. Upward and downward arrows indicate increases and decreases in each parameter, respectively. Bold arrows denote Growth rate and enzyme activity of NanoBiT reporter changes that are consistent with the observed in vivo alterations in MDH1–CIT1 interaction. The color of the parameter and metabolite indicates its effect on MDH1-CIT1 interaction in vitro (blue, inhibitory; red, promotive). αKG, α-ketoglutarate; fum, fumarate; succ, succinate. **(B)** A diagram depicting the proposed regulatory mechanism of the MDH1-CIT1 metabolon association. In conditions with low respiratory flux, the MDH1-CIT1 multienzyme complex dissociates, and the TCA cycle flux reduces. Reduced ETC flux results in higher mitochondrial matrix pH, which reduces MDH1-CIT1 affinity. When the respiratory flux and the TCA cycle flux are high, MDH1-CIT1 metabolon associates and likely channels the intermediate oxaloacetate (OXA). High ETC flux lowers mitochondrial matrix pH and enhances the MDH1-CIT1 interaction. The TCA cycle intermediates affect MDH1-CIT1 metabolon formation; fumarate and malate enhance (red arrows with dotted lines), and citrate inhibits (blue arrows with dotted lines) the interaction. The arrow thickness represents the metabolic fluxes.

The TCA cycle intermediates and cofactors can also regulate the MDH1-CIT1 interaction, considering their effects on the interaction in vitro (Omini et al., 2021). The yeast enzymes showed responses to malate, α-ketoglutarate, succinate, and citrate (Figure 5B, Figure 5 – figure supplement 1) similar to the enzymes of other organisms (Omini et al., 2021; Tompa et al., 1987; Wu et al., 2015), while fumarate is newly identified as an effector of the MDH-CS interaction.

Especially, fumarate, malate, and citrate showed significant influences on yeast enzymes (Figure 5B). Cellular levels of these effector metabolites significantly altered under the conditions tested in this study (Figure 2E, 3M, 4M, 6A). Increased and decreased levels of malate and fumarate following the TCA cycle and ETC inhibitions (Figure 3M&4M), respectively, are likely related to the MDH1-CIT1 interaction since malate enhances the interaction (Figure 5D; Omini et al., 2021). These results indicate the involvement of metabolite effectors, such as malate and fumarate, in the regulation of the MDH1-CIT1 interaction (Figure 6). However, their precise effects must be evaluated through site-specific, time-dependent perturbation and quantification of metabolite levels in the mitochondrial matrix, as a whole-cell metabolite profile may not reflect the metabolite concentrations that directly influence the complex association.

Aside from MDH1-CIT1 interaction dynamics, our results highlight the complex regulation of TCA cycle metabolism. The activation and inhibition of respiratory activity resulted in diverse metabolic phenotypes (Figure 6A, Supplementary Dataset 1), where intermediate levels did not simply reflect overall pathway activity. This complexity stems from the distinct mechanisms of each inhibitor, such as arsenite affecting α-ketoglutarate dehydrogenase and AOA disrupting the malate-aspartate shuttle (Cavero et al., 2003; Eto et al., 1999; Lee et al., 2011; Liu and Butow, 2006), off-target effects of the inhibitors, and from the adaptive reorganization of intersecting metabolic networks to bypass local blockades (Herrgård et al., 2008; Lehtinen et al., 2013; Rogers et al., 2021). These diverse metabolic phenotypes allow us to assess the relationships between metabolites and metabolon assembly independently of respiratory activity.

This study demonstrates that the TCA cycle MDH1-CIT1 multienzyme complex dynamically interacts in response to the cellular respiratory status. Cues of cellular respiratory state may be transmitted to the multienzyme complex, at least in part, by mitochondrial matrix microenvironment and metabolite levels. In particular, mitochondrial matrix pH and malate and fumarate levels likely have significant effects on the stability of the MDH1-CIT1 complex, since these factors strongly influence complex affinity, and their in vivo changes coincide with complex dynamics (Figure 6). However, none of these factors consistently correlates with the MDH1-CIT1 interaction (Figure 6A), suggesting that none of them is a predominant regulator, but multiple factors work together in a cooperative manner to regulate the formation of the multienzyme complex. This coordinated regulation probably serves to fine-tune the flux of the TCA cycle, allowing it to adapt efficiently to varying metabolic demands and maintain cellular homeostasis. Although we focused on allosteric regulators in this study, further factors are potentially involved in the MDH1-CIT1 complex regulation. For example, 44 and 33 post-translational modifications have been identified in CIT1 and MDH1, respectively (Bhagwat et al., 2021; Henriksen et al., 2012; Holt et al., 2009; Lanz et al., 2021; Reinders et al., 2007; Swaney et al., 2013; Weinert et al., 2013), some of which likely affect the MDH1-CIT1 complex affinity. Various scaffolding molecules, such as long noncoding RNAs, lipid layers, and scaffolding proteins, have been shown to stabilize the multienzyme complexes in other systems (Zhu et al., 2022). Future studies should investigate the effects of these factors to understand the regulatory mechanisms for MDH1-CIT1 interaction.

Changes in environmental conditions and nutrient availability occur swiftly, and a corresponding change in metabolic flux must occur at a similar rate for the successful adaptation of living cells. Dynamic metabolons can be a system to regulate and fine-tune metabolic network flux quickly, allowing cells to maintain metabolic homeostasis in rapidly fluctuating environments (Obata, 2019). Considering the thermodynamic unfavorability of the forward MDH reaction and that substrate channeling overcomes this thermodynamic barrier in vitro, the MDH1-CIT1 complex formation likely enhances the forward TCA cycle flux (Bulutoglu et al., 2016; Fukuda et al.,

2008; Sweetlove et al., 2010). The dynamic assembly of the metabolon probably provides fine-tuning of TCA cycle activity in response to respiratory demand. While the present study delineates the environmental and metabolic factors governing this dynamic assembly, future studies utilizing targeted genetic tools to independently modulate specific variables will be critical for dissecting the contributions of individual regulatory factors in vivo. Further studies assessing the impacts of metabolon formation on metabolic pathway flux in living cells are essential to understand the functions of metabolons in metabolic network regulation. Elucidating the regulatory system of the TCA cycle metabolon can lead to a novel strategy to manipulate the TCA cycle flux in metabolic engineering to achieve efficient industrial production of various molecules requiring TCA cycle intermediates as substrates or to control the Warburg effect to suppress cancer cells.

Materials and Methods

Strains, media, and culture conditions

Saccharomyces cerevisiae BY4741 (MATa his3Δ1 leu2Δ0 met15Δ0 ura3Δ0) was used as the background strain. Cells were grown in synthetic complete medium (SD) containing 0.67% yeast nitrogen base lacking amino acids (Research Products International, Mt. Prospect, IL, USA) with 2% w/v D-raffinose and 1% amino acid complete drop-out mix. The complete amino acid drop-out mix was replaced with the amino acid drop-out mix lacking leucine for GoAteam expressing cells or the amino acid drop-out mix lacking uracil for RoGFP and pHluorin expressing cells. Cell growth cultures were incubated with shaking at 220 rpm at 28°C in an incubator shaker. Cell cultures were grown to exponential phase with an OD_{600} = 0.5 to 1.0 in all analyses.

Oxygen consumption rate measurement

Oxygen consumption was measured using a Clark-type electrode (Oxygraph, Hansatech Instruments, Norfolk, UK) as described previously (Agrimi et al., 2011). Cells were grown to exponential phase OD_{600}=0.5, harvested, centrifuged at 3,000 x *g* for 5 min at 4°C, and resuspended in growth medium to obtain a density of OD_{600}=5.0. A total of 1 ml reaction volume consisting of equal parts of 445 µl cell culture, 445 µl growth media, and 10 µl of each inhibitor was added to the oxygraph chamber. Sodium malonate (20 mM), antimycin A (10 µM), sodium cyanide (0.5 mM), and oligomycin (1 mM) were used as specific inhibitors of electron transport chain complex II, III, IV, and V, respectively. The change in oxygen concentration was followed subsequently. Oxygen consumption rates were determined before and after the addition of each inhibitor from the slope of a plot of O_2 concentration versus time. All measurements were conducted in triplicates.

Generation of the *Saccharomyces cerevisiae* reporter strains with tagged MDH1 and CIT1

The NanoBiT split NanoLUC luciferase complementation system (Dixon et al., 2016) was adopted to monitor MDH1-CIT1 interaction in yeast cells. The yeast lines expressing MDH1 and CIT1 proteins fused with the small (SmBiT) and large (LgBiT) NanoBiT subunits, respectively, were generated by inserting the yeast codon-optimized tag-coding sequences into the BY4741 genome following the scarless C-terminal tagging procedure (Landgraf et al., 2016). The full-length NanoLUC, LgBiT, and SmBiT coding sequences were integrated to direct downstream of the Mdh1 (chrIV:3300230) and Cit1 (chrX:303993) genes on the BY4741 genome for C-terminal fusion. The LgBiT and SmBiT sequences include flexible linkers (ACKIPNDLKQKVMNH; (Hu et al., 2002)) with HA and cMyc epitope sequences, respectively, for immunological detections. Details of the vector construction procedure, primers, and vectors are described in the Supplementary Method.

Briefly, we generated the plasmids with integration cassettes composed of the linker, 5' half of tag-coding sequence, URA3 selection marker, and 3' half of tag-coding sequence in this order using the Golden Braid technology (Sarrion-Perdigones et al., 2013). The halves of the tag-coding sequences have an overlapping sequence. The integration cassettes were amplified by PCR using the primers with around 40 bases 5' extension with sequences homologous to the franking region of the tag insertion sites. BY4741 cells were transformed with the purified PCR products to insert

the cassettes into the target sites directly downstream of the Mdh1 and Cit1 genes by homologous recombination due to the 5' extension of the primers. The transformants were selected on uracil-deficient plates. To pop-out the URA3 marker and reconstruct NanoLUC and NanoBiT subunits, the transformants were cultured overnight in uracil-containing YPD media. The URA3 gene was excluded from the genome by recombination based on the overlapping sequences in the cassette. The cell suspension was spread on SD plates containing 1 mg ml^{-1} 5-fluoroorotic acid (5-FOA) to select the cell lines without the URA3 gene. SmBiT was initially fused with the Mdh1 gene, and the resulting strain was further transformed to fuse LgBiT with Cit1 (MDH1/CIT1-BiT strain). Another strain expressing MDH1 fused with full-length NanoLUC luciferase was also generated following the same procedure to monitor MDH1 protein levels (MDH1-nLUC strain).

In vivo MDH1-CIT1 interaction measurement

The MDH1/CIT1-BiT strain expressing MDH1 and CIT1 enzymes tagged with split halves of luciferase enzyme was grown to OD_{600} = 0.35-0.45. Cells were collected and resuspended to obtain a cell density of OD_{600}=2.0 in fresh SD-Raff media. Each sample consisted of 80 µl of media, 10 µl of cells, and 10 µl of 50x furimazine luciferase substrate (Promega, Madison, WI, USA). The luminescence signal was measured every five min with a microplate reader (CLARIOSTAR Plus, BMG LABTECH, Ortenberg, Germany) at 28°C with 200 rpm shaking at the beginning of each cycle. Baseline luminescence was measured for 20 min before the treatment was applied. The time-dependent luminescence was measured for an additional 80 min after treatment. Relative luminescence Unit (RLU) was calculated by normalizing the luciferase signals by the average signals during three pre-treatment time points. The protein levels of MDH1 and CIT1 were assessed using yeast lines expressing these proteins tagged with full-length NanoLUC luciferase. Using the luminescence data of these relative protein levels, we calculated normalized interaction index by dividing the NanoBiT interaction signal by the product of the relative abundances of both proteins:

$$\text{Normalized Interaction Index} = \frac{\text{NanoBiT}}{\text{MDH1} * \text{CIT1}}$$

In this formula, NanoBiT, MDH1, and CIT1 are the relative luminescence levels at each time point.

Western blotting

Cells were grown to OD_{600}=0.5 and cell pellet was collected. Cells were first pretreated with 2 M LiAc and 0.4 M NaOH to permeabilize the cells and then treated with SDS-PAGE sample buffer to extract proteins according to the method described by Zhang et al. (Zhang et al., 2011). The cell lysate was centrifuged at 27,000 x *g* for 10 min at 4°C and the proteins were detected by SDS-PAGE and western blotting following the method described previously (Rajasekaran et al., 2022). cMyc Tag Monoclonal Antibody (MA1213161MG, Thermo Scientific) and HA Tag Monoclonal Antibody (LSG26183, Thermo Fisher Scientific) were used as primary antibodies to detect MDH1 and CIT1, respectively. DLD1 antibody generated by S. Claypool laboratory at the Johns Hopkins University (Baile et al., 2013), and PGK1 Monoclonal Antibody (Invitrogen 459250, Thermo Fisher Scientific) was used to detect phosphoglycerate kinase as a housekeeping protein and internal standard.

In vitro MDH1-CIT1 interaction measurement

The recombinant MDH1 and CIT1 were produced accordingsuw to the method described in the Supplementary Methods. The interaction between recombinant MDH1 and CIT1 enzymes were analyzed by microscale thermophoresis (MST) according to the method described by Omini et al. (Omini et al., 2021) with slight modifications. Base MST buffer contained 50 mM Tris-HCL (pH 8), 150 mM NaCl, 10 mM $MgCl_2$, 5 mM DTT, and 0.05% Tween-20. Recombinant MDH1 (10 µM) was labeled with Protein Labeling Kit RED-NHS 2nd Generation (NanoTemper, München, Germany) and used as the target. CIT1 was used as the ligand. Two-times serial dilution of 80 µM CIT1 was conducted for 16 concentrations. A total of 10 µL of CIT1, 10 µL MST buffer, and 10 µL labeled MDH1 were mixed and loaded to Monolith NT.115 Capillaries (NanoTemper).

Capillaries were incubated at room temperature for 1 min, and the interaction was analyzed by MST using Monolith NT.115 (NanoTemper). To test the effect of pH on MDH1-CIT1 interaction, 50 mM tris buffers with pH 6.0, 7.5, and 8.0 were prepared and used as the MST buffer for sample preparation. To test the effect of reducing environment on interaction, various concentrations (5 mM, 2.5 mM, 1.25 mM) of DTT were prepared with the MST buffer and used for sample preparation. To test the effect of ATP level on interaction, an MST buffer containing different concentrations of ATP (5 mM, 2.5 mM, 1.25 mM) was made and used for sample preparation. To test the effect of metabolite availability on the interaction, MST buffer containing respective metabolites at 10 mM concentration was made and used for sample preparation and experiments.

Enzyme activity assays

Cells were grown to an exponential phase with OD_{600} of 0.5, and 2 ml of the cells were harvested for enzyme activity assay. Yeast cell lysates were prepared by disruption with glass beads as described previously (Mukherjee et al., 2020), with the lysis buffer omitted butylhydroxytoluene. The protein concentration of the lysate was determined using Pierce™ BCA Protein Assay Kit (Thermo Fischer Scientific). CS activity was determined using a method described previously (Srere, 1969) that measures free thiols by coupling the citrate synthase reaction to thiol reaction with 5, 5'-dithiobis-(2-nitrobenzoate) (DTNB). The CS enzyme activity assay mixture contained 154 µL of distilled water, 20 µL of 1 mM DTNB, and 6 µL of 10 mM acetyl CoA. The citrate synthase reaction was initiated by the addition of 10 µL of 10 mM oxaloacetate. The absorption at 412 nm was followed to measure citrate synthase activity. MDH activity assay mixture contained 50 mM TES (pH 7.2), 5 mM $MgCl_2$, 0.2 mM NADH, and 0.05% Triton X100. To obtain a total reaction volume of 300 µL, 285 µL of the assay mixture and 5 µL cell lysate were added to the wells, and the reaction was initiated with 10 µL of 30 mM oxaloacetate. Reduction of NADH was followed at 340 nm to determine MDH enzyme activity. Enzyme activity was measured using a microplate reader absorbance function (CLARIOSTAR Plus, BMG LABTECH).

Metabolite profiling

Yeast cells were grown to the exponential phase (OD_{600}~0.5), and treatments were applied and incubated for the time described in the figure legends. Cellular metabolites were extracted following the protocol described by Obata et al. (Obata et al., 2013). The cells in 1 mL culture were harvested by vacuum filtration using a membrane filter (0.45 µm HV Durapore 25 mm diameter; MilliporeSigma, Burlington, MA, USA). The filter was put into a 2 mL microcentrifuge tube, flash-frozen in liquid nitrogen, and stored at −80°C. The metabolites were extracted from the filtered cells with methanol: water: chloroform, and 50 µL aliquot was dried down by vacuum centrifugation. Dried metabolites were derivatized with methoxyamine hydrochloride in pyridine and further trimethylsylilated by N-Methyl-N-(trimethylsilyl) trifluoroacetamide (MilliporeSigma). Derivatized samples were analyzed by 7200 GC-QTOF system (Agilent, Santa Clara, CA, USA) exactly as described in Wase et al. (Wase et al., 2022). Each metabolite's peak height was normalized by the peak height of the internal standard (ribitol) to represent relative levels of metabolite.

Expression of mitochondrial biosensors

The pH, redox state, and ATP levels in the mitochondrial matrix were measured using the mito-Go Ateam2, mito-ROGFP1, and pHluorin (pAG416-COX4-pHluorin, URA selection marker) fluorescence biosensors, respectively, specifically localizing in the mitochondrial matrix. The mito-Go Ateam2 (p415-GPDpro-mito GO ATeam) and mito-roGFP1 (p416-GPDpro-mito roGFP) encoding plasmids (Vevea et al., 2013) were generous gifts from Dr. Liza Pon at Department of Pathology and Cell Biology, Columbia University. The pHluorin encoded plasmid (pAG416-COX4-pHluorin;(Ayer et al., 2013)) was a generous gift from Dr. Anita Ayer at the University of New South Wales, Sydney, Australia. The plasmids encoding these biosensors were transformed into split-Luc tagged

MDH1/CIT1 strain using the lithium acetate method (Chen et al., 1992). The p416-GPDpro-mito roGFP and pAG416-COX4-pHluorin harboring cells were selected on URA- media, and the cells with p415-GPDpro-mito GO ATeam were selected on Leu- media.

The localization of biosensors within the mitochondria was confirmed by confocal microscopy. Cells were grown in SD selection media to OD_{600}=0.50. Cells were stained with MitoTracker Deep Red FM (ThermoFisher Scientific) in a 100 nM dye solution for 30 min with shaking at 28 °C to visualize the mitochondria. The stained cells were resuspended in fresh 10 mM HEPES buffer (pH 7.4) with 2% raffinose to obtain a final concentration of OD_{600}=10. Confocal imaging was performed on an A1R-Ti2 Confocal Laser Scanning Microscope (Nikon, Tokyo, Japan) with a Plan Apo 60x 1.40 Oil lens 0.17 WD 0.13 (Nikon) and a 2x digital zoom for a total magnification of 1200x. Brightfield and fluorescent images were captured. Imaging was done sequentially with excitation at 405 nm and emission at 425-475 nm for pHluorin and mito-roGFP1, excitation at 488 nm and emission at 500-550 nm for mito-GoAteam2, and excitation at 640 nm and emission at 663-738 nm for MitoTracker. Images were collected with NIS Elements software (Nikon) and processed with ImageJ analysis software (Vevea et al., 2013).

Measurement of redox state, pH, and ATP level in the mitochondrial matrix

Cells expressing pHluorin, mito-roGFP1, and mito-GoAteam2 were grown to OD_{600}=0.50 in their respective selection media. Cells were prepared for fluorescence measurement according to the method described by Morgan *et al* (Morgan et al., 2011). Time-based fluorescence intensity was measured using a microplate reader (CLARIOSTAR Plus, BMG LABTECH) at 28°C with shaking at 200 rpm with 20 min of baseline measurement before treatments. In all experiments, the strains harboring empty vectors were grown simultaneously as a reference for background fluorescence at the different excitation wavelengths. Background fluorescence was subtracted from fluorescence intensity from cells expressing biosensors.

For the pH measurement, the ratio of emission intensity at 510 nm resulting from excitation of pHluorin at 390 nm and 470 nm was calculated (R390/470) using pHluorin expressing strain. The mitochondrial matrix pH was calculated from the R390/470 ratio using a calibration curve generated according to the method described by Orij *et al* (Orij et al., 2009). Briefly, pHluorin-expressing cells were permeabilized by resuspension in PBS containing 100 µg ml-1 digitonin for 10 min and washed with PBS. Cells were resuspended in citric acid/Na2HPO4 buffer of pH values ranging from 5.0 to 9.0. The ratio of pHluorin emission at 510 nm upon excitation at 390 and 470 nm (R390/470) was plotted against buffer pH to obtain a calibration curve.

The mitochondrial matrix redox state was measured using mito-roGFP1 expressing strain. The ratio of emission intensity at 510 nm from excitation at 365 nm and 470 nm (R470/365) was measured. Mito-roGFP1 in situ calibration was performed following the method described by (Vevea et al., 2013). Digitonin-treated mito-roGFP1 expressing cells were incubated in 0, 5, and 10 mM H_2O_2 and DTT for 20 min at 28°C with shaking at 200 rpm. The R470/365 was plotted against the redox potential of the solutions calculated using the formula described previously (Morgan et al., 2011).

Relative ATP level was determined by measuring the ratio of the emission intensity of mito-GoAteam2 at 510 nm and 560 nm with excitation at 470 nm (R560/510). The ATP levels were analyzed as the relative value without calibration to absolute concentrations.

Statistical Analysis

The differences between the control and test samples were evaluated by a two-tailed unpaired Student's *t*-test. $p < 0.05$ was considered a statistically significant difference. For the time course data, the test was applied at each time point. All data was obtained from triplicated independent experiments.

Figure supplements

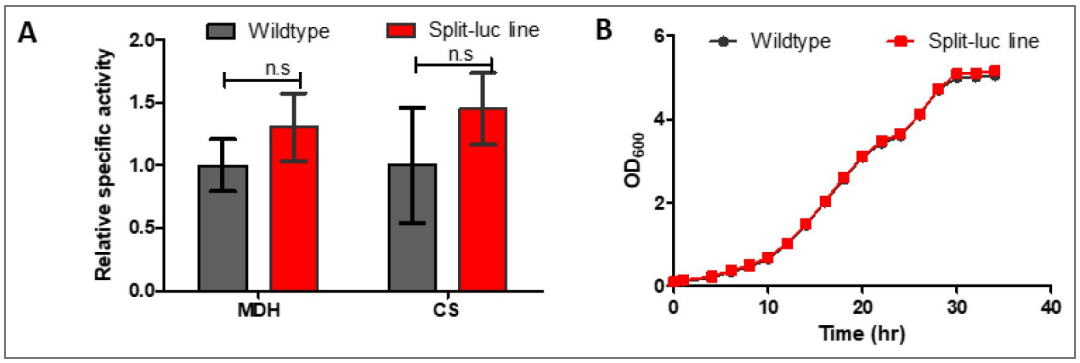

Figure 1 – figure supplement 1. Growth rate and enzyme activity of NanoBiT reporter strain. (A) Extractable cellular MDH and CS enzyme activities in the wildtype (black) and NanoBiT reporter strain (Split-luc line, red). (B) Growth of cells in SD-raff media monitored as culture OD600. Data is presented as mean ± s.d. Statistical differences against the wildtype samples were assessed by Student's *t*-test at each time point. n.s., not significant ($p>0.05$).

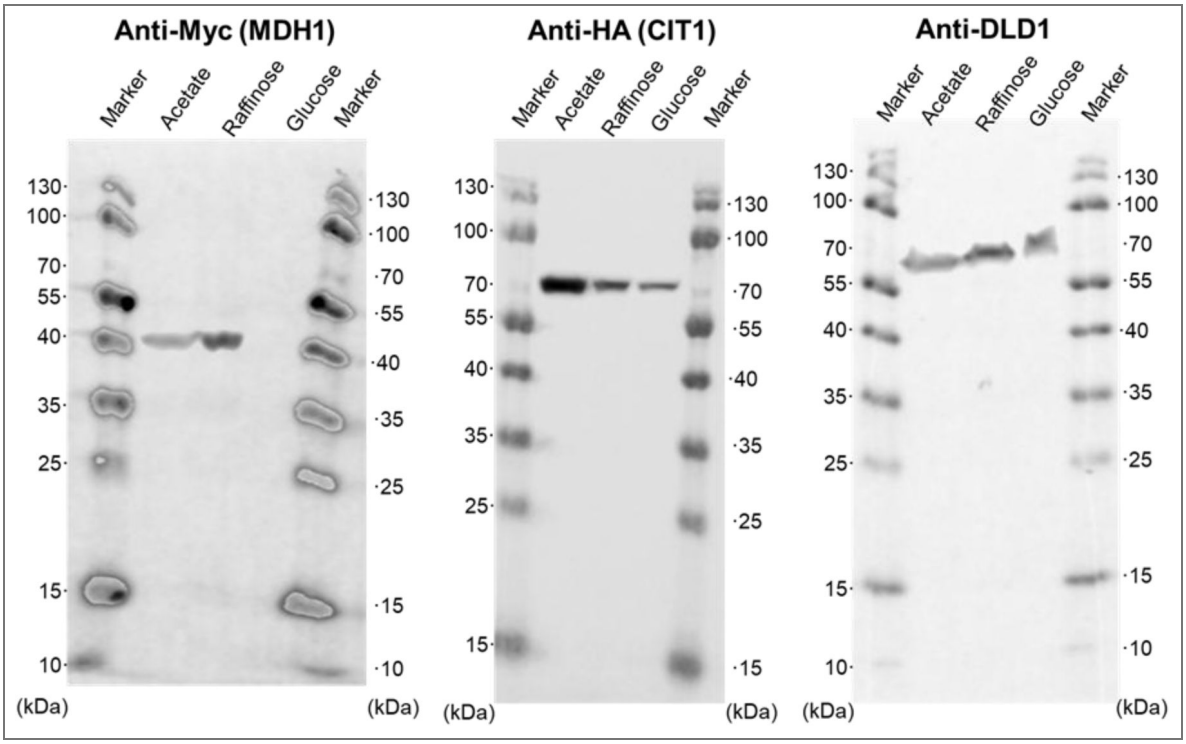

Figure 1 – figure supplement 2. Full Western blotting image showing MDH1 and CIT1 protein abundance in Figure 1C.

The numbers on the side of the images indicate the size of the molecular weight markers (kDa).

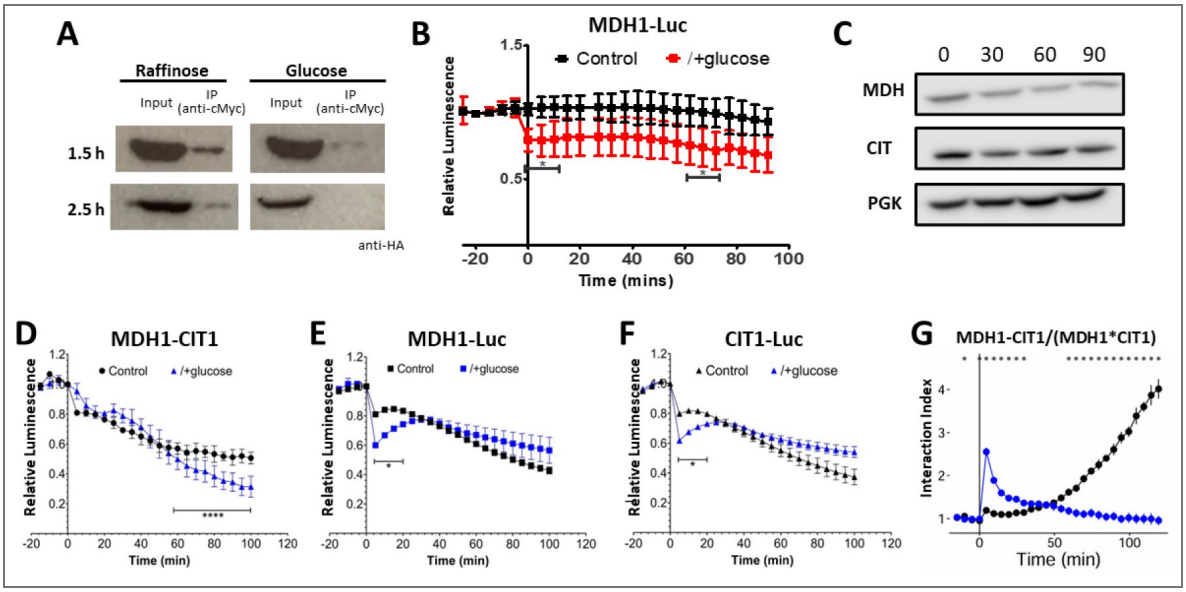

Figure 2 – figure supplement 1. MDH1-CIT1 interaction and protein abundance following the application of glucose.

(A) Co-immunoprecipitation of CIT1 with MDH1. In the Split-luc line, MDH1-LgBiT and CIT1-SmBiT harbor cMyc and HA tag in the linker sequence. Proteins were extracted from the Split-luc line grown in SD-faff media at 1.5 and 2.5 hours following 2% glucose application. MDH1 was precipitated with anti-cMyc agarose and co-precipitated CIT1 was detected by anti-HA antibody following SDS-PAGE separation. **(B)** MDH1 protein levels monitored by the luminescence of MDH1 fused with full-length NanoLUC luciferase. **(C)** Western blot analysis of MDH1 and CIT1 protein levels after 0, 30, 60, and 90 min of Crabtree induction. Phosphoglycerate kinase (PGK) was detected as a loading control. **(D)** NanoBIT signal indicating MDH1-CIT1 interaction in a repeated glucose supplementation experiment. SD-Raff-grown cells were treated with 2% glucose at 0 min (blue). **(E)** MDH1 protein levels monitored by the luminescence of MDH1 fused with full-length nanoLUC luciferase in the repeated experiment. **(F)** MDH1 protein levels monitored by the luminescence of CIT1 fused with full-length nanoLUC luciferase in the repeated experiment. Relative luminescence was calculated by normalizing the luciferase signals by the average signals during three pre-treatment time points. Statistical differences against the control samples were assessed by Student's *t*-test at each time point (N=4). Asterisks indicate significant difference (*, $p<0.05$; ****, $p<0.0001$; ns, not significant). **(G)** Interaction index calculated by normalizing NanoBiT signal by those of MDH1-nanoLUC and CIT1-nanoLUC. Asterisks indicate time points with statistically significant differences (p<0.05) between control and glucose conditions (N=4).

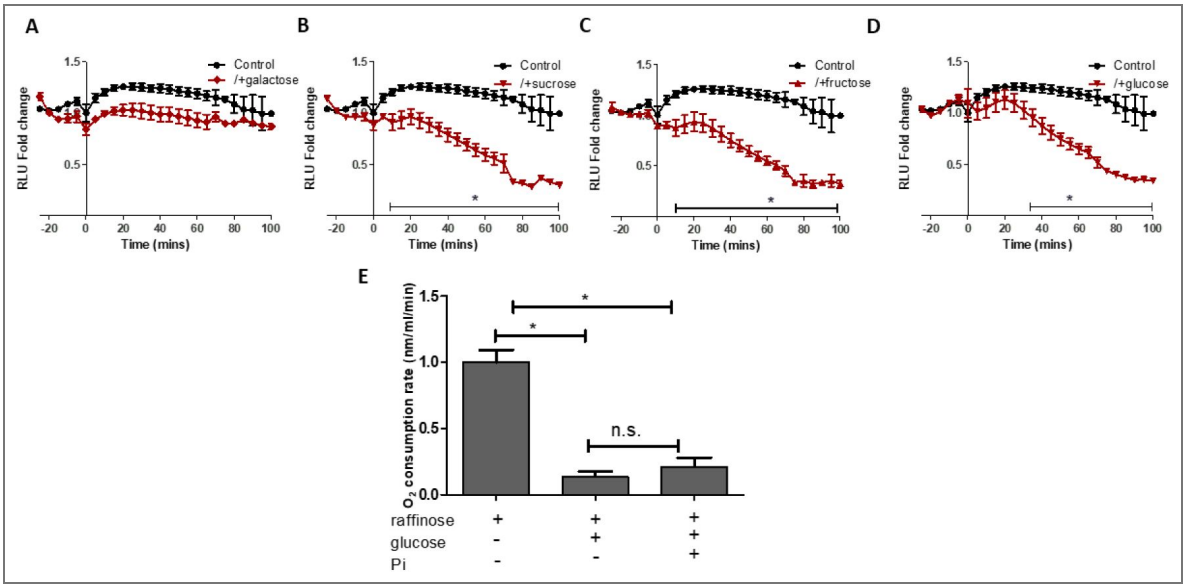

Figure 2 – figure supplement 2. Effects of sugars on MDH1-CIT1 complex assembly and oxygen consumption rate.

(A-D) NanoBiT signal indicating effect of galactose, sucrose, fructose, and glucose on MDH1-CIT1 interaction. Cells were cultured in fresh SD-Raff media in the control condition (black). The cells are treated with 2% sugar application to the SD-Raff-grown cells at 0 min (red). Relative luciferase unit (RLU) was calculated by normalizing the luciferase signals by the average signals during three pre-treatment time points. **(E)** Effects of glucose and inorganic phosphate (fermentation inhibitor) on oxygen consumption rate. Basal O_2 consumption rate of SD-Raff grown cells was measured. Glucose and inorganic phosphate were added and O_2 consumption rate was measured for 5 minutes. All data in A-E are presented as mean ± s.d. Statistical differences against the control samples were assessed by Student's *t*-test at each time point (N=4). Asterisks indicate significant differences with $p<0.05$.

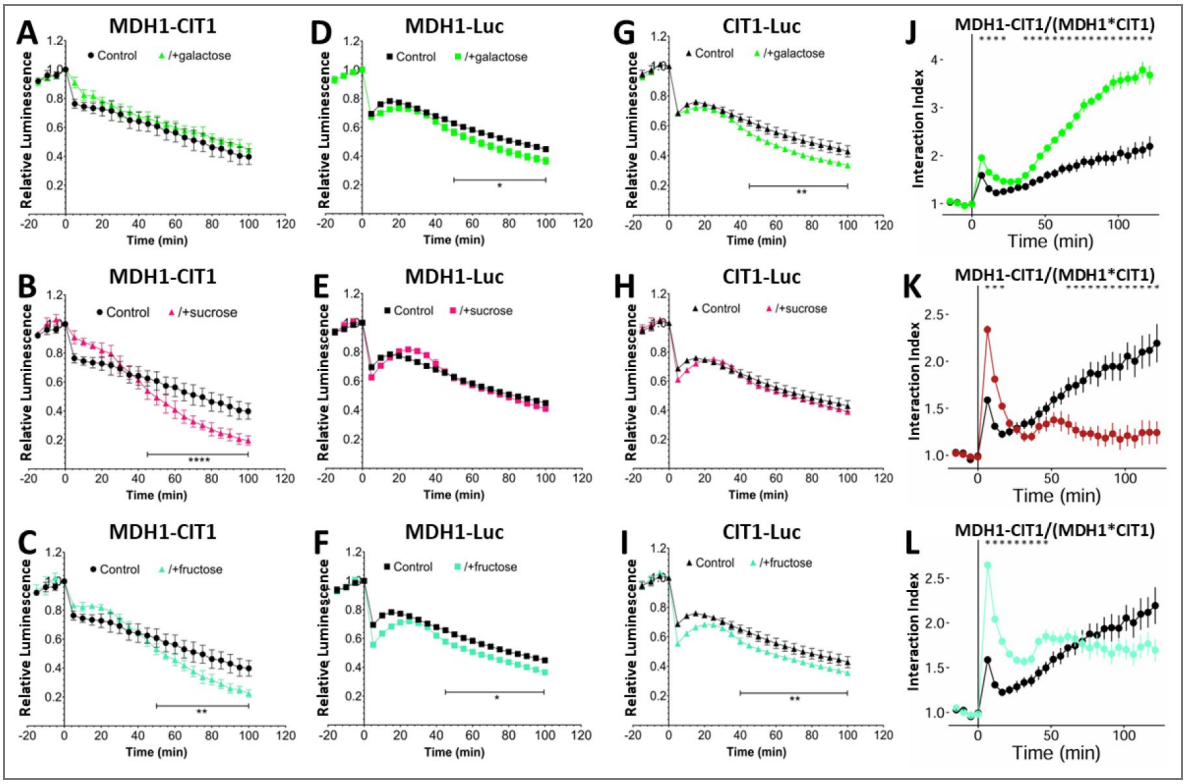

Figure 2 – figure supplement 3. Repeated experiments investigating the effects of sugars on MDH1-CIT1 complex assembly and MDH1 and CIT1 protein abundance following the addition of galactose (green), sucrose (magenta), and fructose (cyan).

(A-C) NanoBIT signal indicating effect of galactose **(A)**, sucrose **(B)**, and fructose **(C)** on MDH1-CIT1 interaction. Cells were cultured in fresh SD-Raff media in the control condition (black). The cells are treated with 2% sugar application to the SD-Raff-grown cells at 0 min. Relative luciferase unit (RLU) was calculated by normalizing the luciferase signals by the average signals during three pre-treatment time points. **(D-F)** MDH1 protein levels monitored by the luminescence of MDH1 fused with full-length NanoLUC luciferase. **(G-I)** CIT1 protein levels monitored by the luminescence of CIT1 fused with full-length nanoLUC luciferase. Relative luminescence was calculated by normalizing the luciferase signals by the average signals during three pre-treatment time points. Statistical differences against the control samples were assessed by Student's *t*-test at each time point (N=4). Asterisks indicate significant differences (*, $p<0.05$; **, $p<0.01$; ****, $p<0.0001$). **(J-L)** Interaction index calculated by normalizing NanoBiT signal by those of MDH1-NanoLUC and CIT1-NanoLUC.

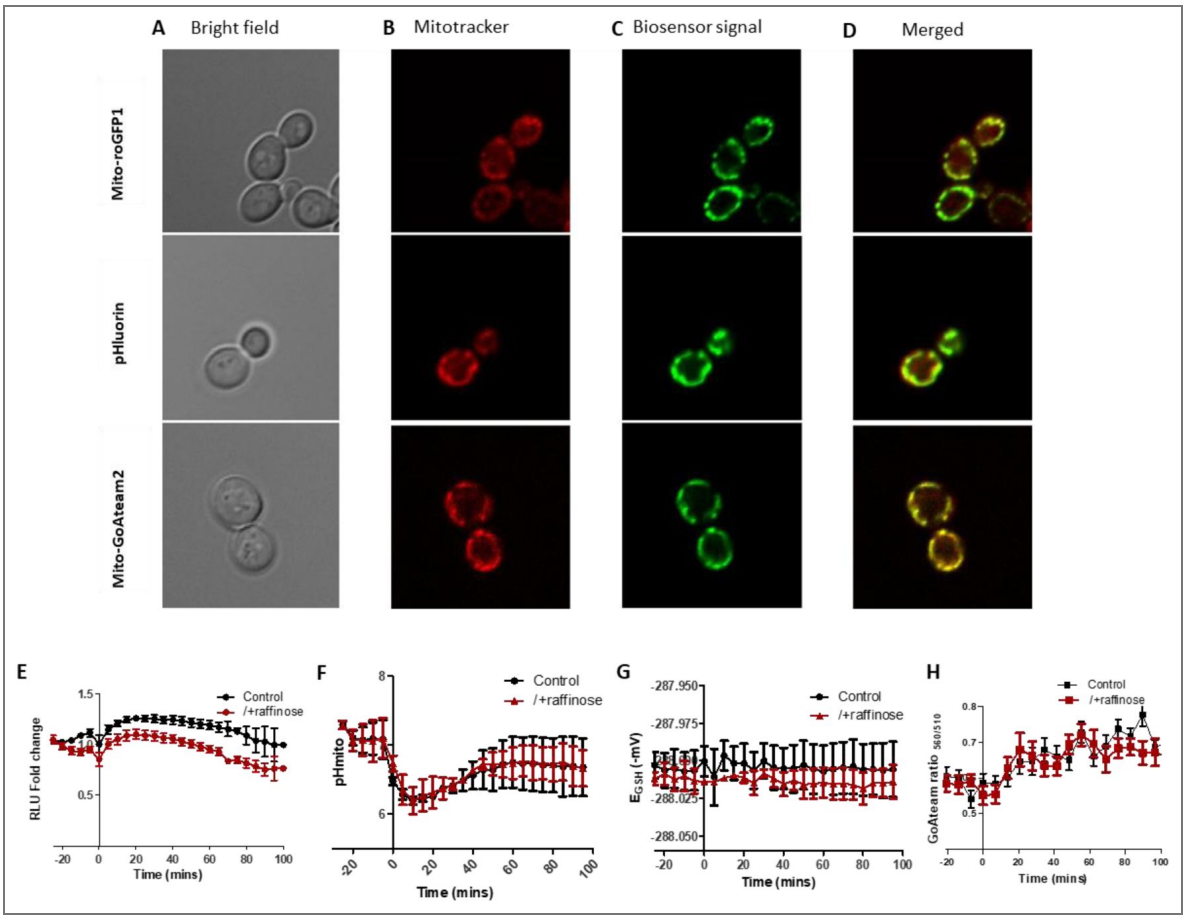

Figure 2 – figure supplement 4. Biosensors indicate mitochondria microenvironments.

(A-D) Subcellular localizations of fluorescent biosensors. The yeast strains expressing Mito-roGFP1 (upper panels), pHluorin (middle panels), and Mito-GoAteam2 (lower panels) were observed by fluorescent microscopy in the SD-Raff media. The cells were stained with Mitotracker orange prior to the analysis. **(A)** Bright field image. **(B)** Mito tracker signal. **(C)** Biosensor signals. **(D)** Merged images of the A to C. **(E)** Effect of raffinose addition on MDH1-CIT1 interaction. Cells were cultured in SD-Raff media in the control condition (black). The cells are applied with 2% raffinose to the SD-Raff-grown cells at 0 min (red). Relative luciferase unit (RLU) was calculated by normalizing the luciferase signals by the average signals during three pre-treatment time points. **(F)** Mitochondrial matrix pH in control cells (black) and cells applied with additional raffinose (red). **(G)** Mitochondrial matrix redox state reported as redox potential of roGFP1 (mV). **(H)** Mitochondrial matrix ATP level indicated by the ratio between 560 and 510 nm emission signals of mito-GoATeam2 sensor. Data in E-H are presented as mean ± s.d. (N=4). No statistical difference was detected between the control and raffinose cells.

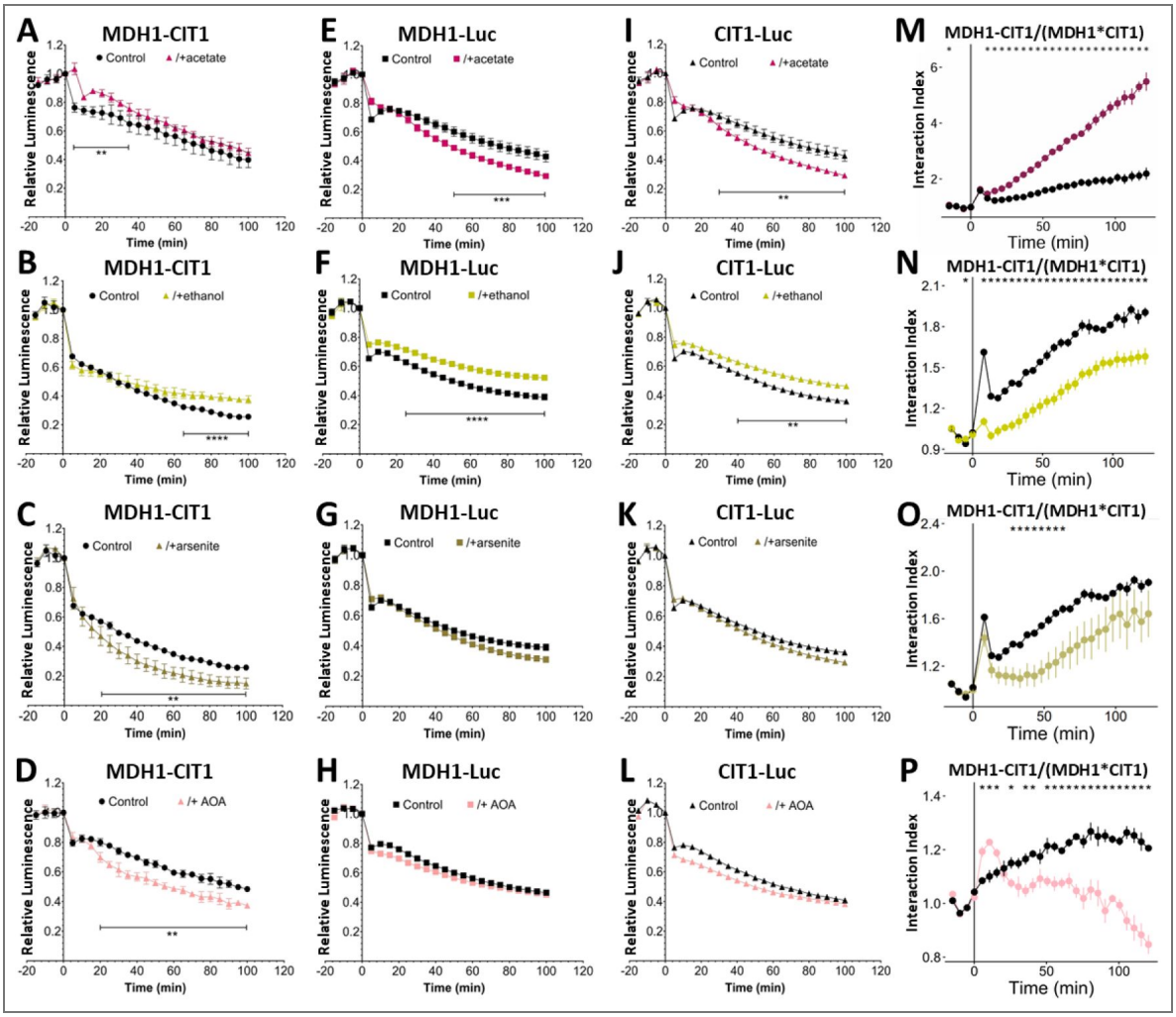

Figure 3 – figure supplement 1. MDH1-CIT1 complex association and MDH1 and CIT1 protein levels following TCA cycle activation and inhibition (repeated experiment).

Cells were cultured in SD-Raff media in the control condition (black). The TCA cycle activator (acetate, dark red; ethanol, light yellow) and inhibitors (arsenite, dark yellow; aminooxyacetate, AOA, pink) were applied at 0 min. **(A-D)** NanoBIT signal indicating the MDH1-CIT1 interaction. **(E-H)** MDH1 protein levels monitored by the luminescence of MDH1 fused with full-length NanoLUC luciferase. **(I-L)** CIT1 protein levels monitored by the luminescence of CIT1 fused with full-length NanoLUC luciferase. Relative luminescence Unit (RLU) was calculated by normalizing the luciferase signals by the average signals during three pre-treatment time points. Statistical differences against the control samples were assessed by Student's *t*-test at each time point (N=4). Asterisks indicate significant differences (**, $p<0.01$; ***, $p<0.001$). **(M-P)** Interaction index calculated by normalizing NanoBiT signal by those of MDH1-NanoLUC and CIT1-NanoLUC. Asterisks indicate time points with statistically significant differences ($p<0.05$) between control and treatment conditions (N=4).

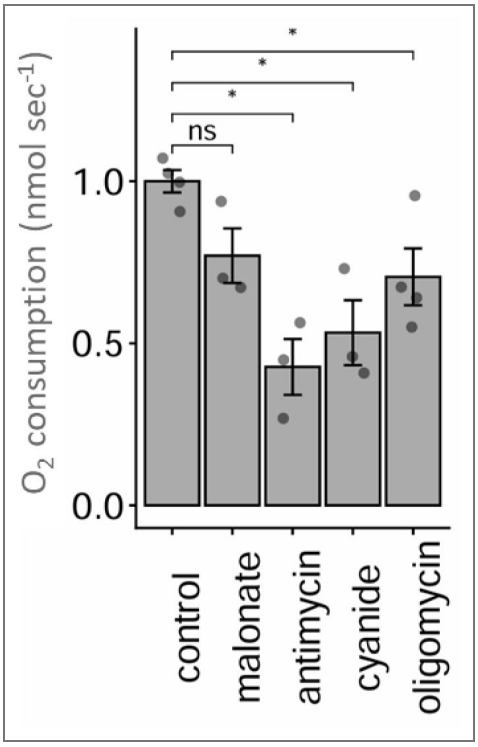

Figure 4 - figure supplement 1. **Effect of ETC inhibitors on O_2 consumption rate.**

Basal O_2 consumption rate was measured, then inhibitor was added and O_2 consumption rate was measured for 5 minutes. Data is presented as mean ± s.d. (N=4), Statistical differences against the control samples were assessed by Student's *t*-test. Asterisks indicate significant differences with $p<0.05$.

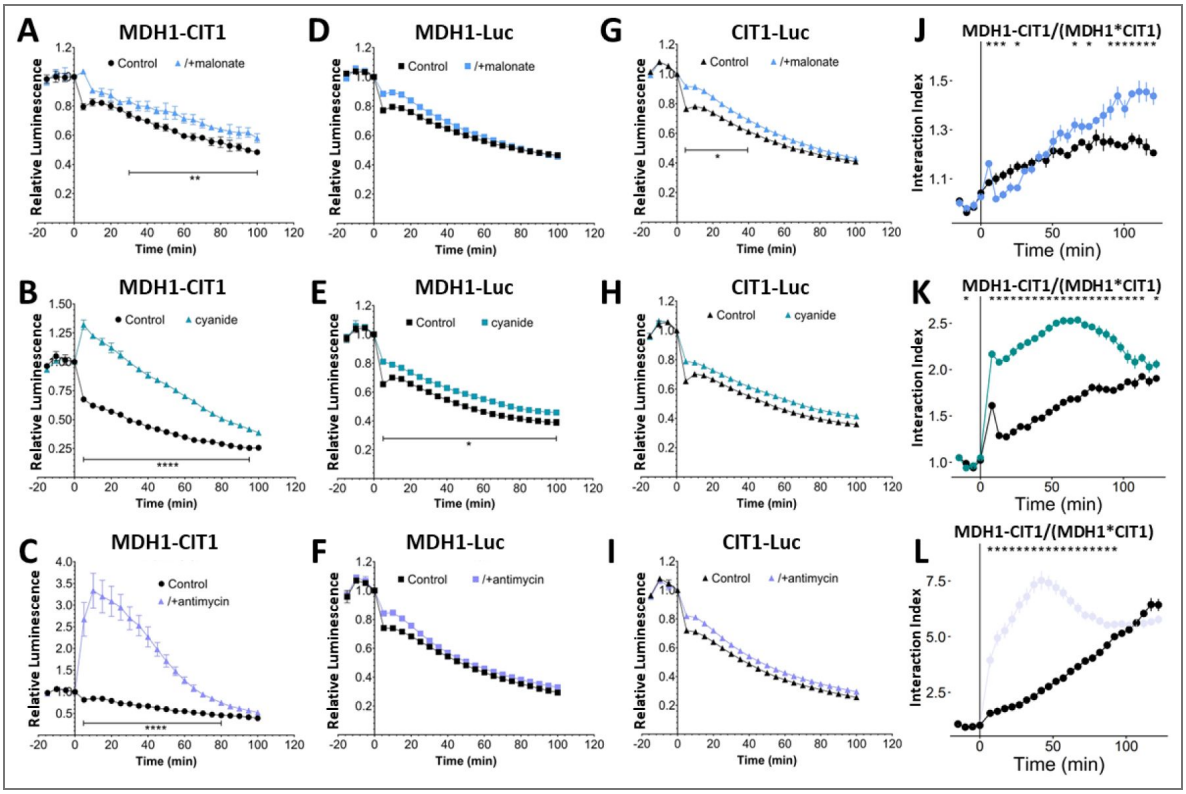

Figure 4 - figure supplement 2. Effect of ETC inhibitors on MDH1-CIT1 complex association and MDH1 and CIT1 protein levels (repeated experiment).

Cells were cultured in SD-Raff media in the control condition (black). The electron transport chain inhibitors (malonate, light blue; cyanide, cyan; antimycin, light purple) were applied at 0 min. **(A-C)** NanoBIT signal indicating MDH1-CIT1 interaction. **(D-F)** MDH1 protein levels monitored by the luminescence of MDH1 fused with full-length NanoLUC luciferase. **(G-I)** CIT1 protein levels monitored by the luminescence of CIT1 fused with full-length NanoLUC luciferase. Relative luminescence Unit (RLU) was calculated by normalizing the luciferase signals by the average signals during three pre-treatment time points. Statistical differences against the control samples were assessed by Student's *t*-test at each time point (N=4). Asterisks indicate significant differences (*, $p<0.05$; **, $p<0.01$; ****, $p<0.0001$). **(J-L)** Relative luminescence of the NanoBiT signal normalized by those of MDH1-NanoLUC and CIT1-NanoLUC. Asterisks indicate the time points with statistical significance ($p<0.05$) between control and treatment conditions.

Figure 4 – figure supplement 3. Effects of Complex V inhibition on MDH1-CIT1 complex association, mitochondrial microenvironments, and cellular metabolite levels.

Cells were cultured in SD-Raff media in the control condition (black). Oligomycin was applied at 0 min (red). **(A)** NanoBiT signal indicating MDH1-CIT1 interaction. Relative luciferase unit (RLU) was calculated by normalizing the luciferase signals by the average signals during three pre-treatment time points. **(B)** Mitochondrial matrix pH. **(C)** Mitochondrial matrix redox states as GSH/GSSG equivalent (mV). **(D)** Mitochondrial matrix ATP level indicated by the ratio between 560 and 510 nm emission signals of mito-GoATeam2 sensor. All data in A-D are presented as mean ± s.d. (N=4). **(E)** Cellular metabolite levels after 80 min of oligomycin treatment. The boxes, lines, error bars, and points indicate interquartile range, median, minimum, and maximum values, and outliers, respectively. Statistical differences against the control samples were assessed by Student's *t*-test (N=3). No statistical difference was detected between control and oligomycin-treated cells.

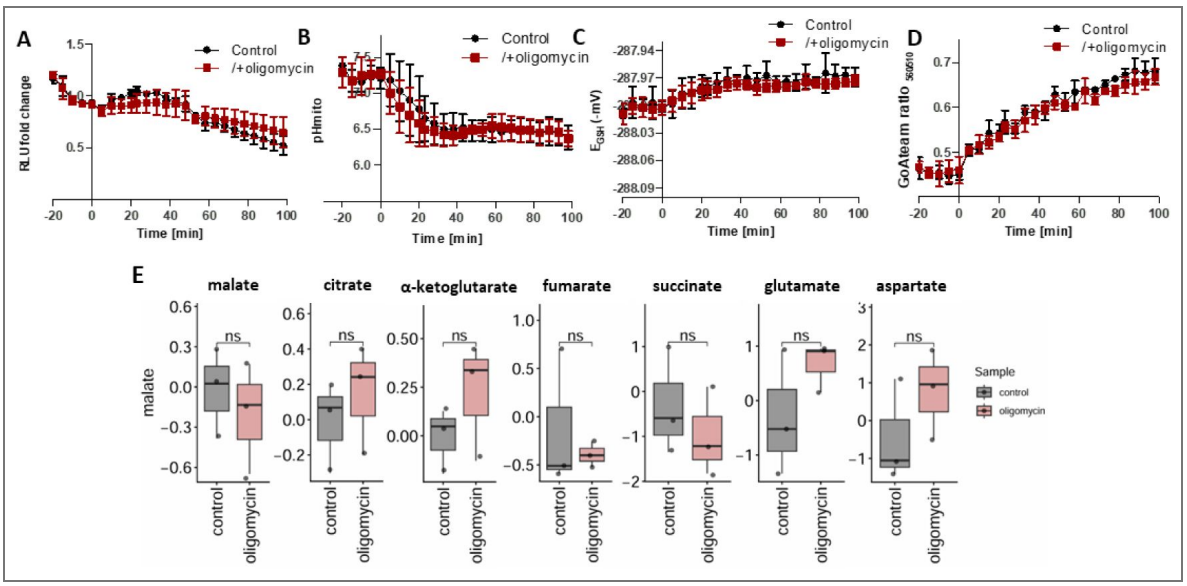

Figure 4 – figure supplement 4. MDH1-CIT1 complex association and MDH1 and CIT1 protein levels following oxidative phosphorylation uncoupler (carbonyl cyanide 3-chlorophenylhydrazone; CCCP) application.

Cells were cultured in SD-Raff media in the control condition (black). CCCP (dark red) were applied at 0 min. **(A)** NanoBIT signal indicating MDH1-CIT1 interaction. **(B)** MDH1 protein levels monitored by the luminescence of MDH1 fused with full-length NanoLUC luciferase. **(C)** CIT1 protein levels monitored by the luminescence of CIT1 fused with full-length NanoLUC luciferase. Relative luminescence Unit (RLU) was calculated by normalizing the luciferase signals by the average signals during three pre-treatment time points. Statistical differences against the control samples were assessed by Student's *t*-test at each time point (N=4). Asterisks indicate significant differences (**, $p<0.01$; ****, $p<0.0001$). **(D)** Interaction index calculated by normalizing NanoBiT signal by those of MDH1-NanoLUC and CIT1-NanoLUC. Asterisks indicate time points with statistically significant differences ($p<0.05$) between control and CCCP conditions (N=4).

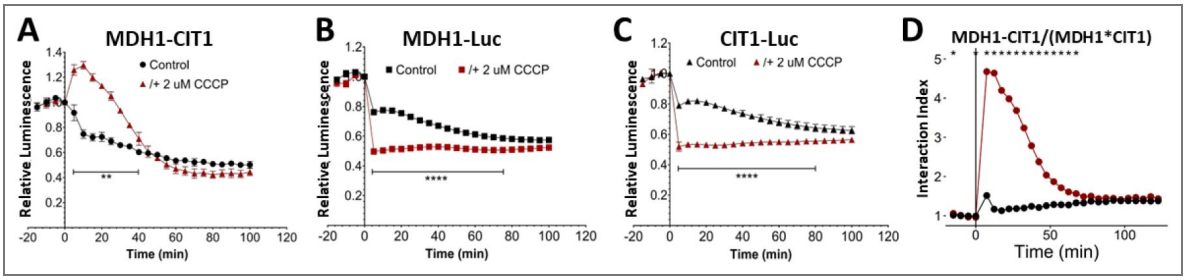

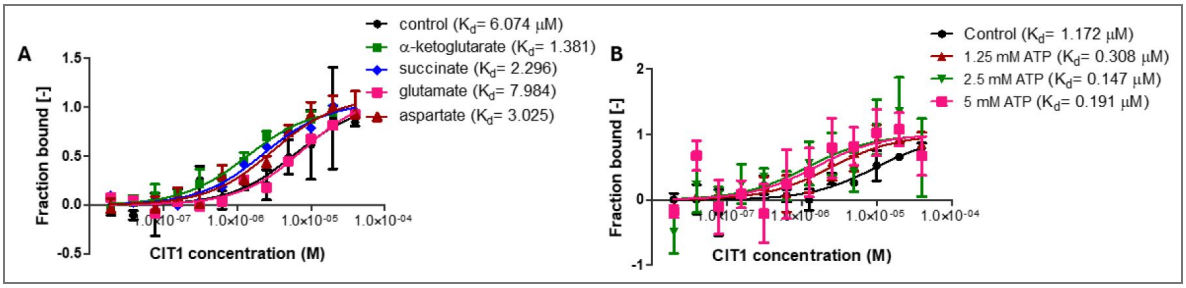

Figure 5 – figure supplement 1. The affinity of the MDH1-CIT1 multienzyme complex was analyzed by microscale thermophoresis (MST) using fluorescently labeled MDH1 as the target and CIT1 as the ligand.

Curves represent the response (fraction bound) against CIT1 concentration. Points represent the means of fraction bound, and the error bars represent the standard deviations of three measurements (N=3). **(A)** Effects of metabolites. The MDH1-CIT1 interaction was determined in the buffer (control; black) with 10 mM α-ketoglutarate (green), 10 mM succinate (blue), 10 mM glutamate (pink), and 10 mM aspartate (dark red). **(B)** Effects of 1.25 mM (brown), 2.5 mM (green), and 5 mM (pink) ATP. The K_d values of MDH1-CIT1 interaction were shown next to the legend.

Data availability

All data generated or analyzed during this study are included in the manuscript and supporting files. The dataset for the metabolite profiling is provided in Supplementary Dataset 1.

Acknowledgements

This study is supported by the NSF CAREER Award to TO under Grant No. 1845451. Dr. Liza Pon at Columbia University kindly gifted us the mito-Go Ateam2 and mito-ROGFP1 biosensors, and Dr. Anita Ayer at the University of New South Wales, Sydney, Australia, gifted us the pHluorin mitochondrial biosensor. Dr. Oleh Khalimonchuk at the University of Nebraska-Lincoln provided us with the anti-DLD1 antibody. The Microscopy work assisted by Terri Fangman was carried out at the Microscopy Research Core Facility of the Center for Biotechnology at the University of Nebraska-Lincoln, which is partially funded by the Nebraska Center for Integrated Biomolecular Communication COBRE grant (P20 GM113126 and NIGMS) and the Nebraska Research Initiative. This paper is based on a dissertation submitted by Joy Omini to fulfill the requirements for the degree of Doctor of Philosophy, University of Nebraska-Lincoln (Omini, 2024).

Additional files

Supplementary Dataset 1 Metabolite profiling data of the *S. cerevisiae* cells. The relative metabolite levels were used for the analyses in this study. The raw peak heights, quantitative ion m/z, and the retention time of the each analyzed peak are also indicated. The metabolite profiling was conducted in two batchs. CONTROL1, GLUCOSE, CYANIDE, ACETATE, ARSENITE, and AOA conditions were analyzed in the first batch (N=7). CONTROL2, MALONATE, OLIGOMYCIN, and ANTIMYCIN were analyzed in the second batch (N=3).

Supplementary Method

Additional information

Funding

Funder	Grant reference number	Author
National Science Foundation (NSF)	1845451	Toshihiro Obata

Author ORCID iDs

Taiwo Dele-Osibanjo: https://orcid.org/0000-0003-2537-6998
Toshihiro Obata: https://orcid.org/0000-0001-8931-7722

References

1. **Agrimi G,** Brambilla L, Frascotti G, Pisano I, Porro D, Vai M, Palmieri L (2011) Deletion or Overexpression of Mitochondrial NAD + Carriers in Saccharomyces cerevisiae Alters Cellular NAD and ATP Contents and Affects Mitochondrial Metabolism and the Rate of Glycolysis. *Applied and Environmental Microbiology* **77**:2239-2246 https://doi.org/10.1128/AEM.01703-10 | PubMed
2. **Ahmadzadeh M,** Horng A, Colombini M (1996) The control of mitochondrial respiration in yeast: A possible role of the outer mitochondrial membrane. *Cell Biochemistry and Function* **14**:201-208 https://doi.org/10.1002/cbf.673 | PubMed
3. **Ayer A,** Sanwald J, Pillay BA, Meyer AJ, Perrone GG, Dawes IW (2013) Distinct Redox Regulation in Sub-Cellular Compartments in Response to Various Stress Conditions in Saccharomyces cerevisiae. *PLOS One* **8**:e65240 https://doi.org/10.1371/journal.pone.0065240 | PubMed

4. **Baile MG,** Whited K, Claypool SM (2013) Deacylation on the matrix side of the mitochondrial inner membrane regulates cardiolipin remodeling. *Molecular Biology of the Cell* **24**:2008-2020 https://doi.org/10.1091/mbc.e13-03-0121 | PubMed

5. **Beeckmans S** (1984) Some structural and regulatory aspects of citrate synthase. *International Journal of Biochemistry* **16**:341-351 https://doi.org/10.1016/0020-711X(84)90131-9 | PubMed

6. **Beeckmans S,** Kanarek L (1981) Demonstration of Physical Interactions between Consecutive Enzymes of the Citric Acid Cycle and of the Aspartate-Malate Shuttle. *European Journal of Biochemistry* **117**:527-535 https://doi.org/10.1111/j.1432-1033.1981.tb06369.x | PubMed

7. **Bhagwat NR,** Owens SN, Ito M, Boinapalli J V, Poa P, Ditzel A, Kopparapu S, Mahalawat M, Davies OR, Collins SR, *et al.* (2021) SUMO is a pervasive regulator of meiosis. *eLife* **10** https://doi.org/10.7554/eLife.57720 | PubMed

8. **Borst P** (2020) The malate–aspartate shuttle (Borst cycle): How it started and developed into a major metabolic pathway. *IUBMB Life* **72**:2241-2259 https://doi.org/10.1002/iub.2367 | PubMed

9. **Bulutoglu B,** Garcia KE, Wu F, Minteer SD, Banta S (2016) Direct Evidence for Metabolon Formation and Substrate Channeling in Recombinant TCA Cycle Enzymes. *ACS Chemical Biology* **11**:2847-2853 https://doi.org/10.1021/acschembio.6b00523 | PubMed

10. **Causton HC,** Ren B, Koh SS, Harbison CT, Kanin E, Jennings EG, Lee TI, True HL, Lander ES, Young RA (2001) Remodeling of Yeast Genome Expression in Response to Environmental Changes. *Molecular Biology of the Cell* **12**:323-337 https://doi.org/10.1091/mbc.12.2.323 | PubMed

11. **Cavero S,** Vozza A, Del Arco A, Palmieri L, Villa A, Blanco E, Runswick MJ, Walker JE, Cerdán S, Palmieri F, *et al.* (2003) Identification and metabolic role of the mitochondrial aspartate-glutamate transporter in Saccharomyces cerevisiae. *Molecular Microbiology* **50**:1257-1269 https://doi.org/10.1046/j.1365-2958.2003.03742.x | PubMed

12. **Chen D-C,** Yang B-C, Kuo T-T (1992) One-step transformation of yeast in stationary phase. *Current Genetics* **21**:83-84 https://doi.org/10.1007/BF00318659 | PubMed

13. **Diaz-Ruiz R,** Rigoulet M, Devin A (2011) The Warburg and Crabtree effects: On the origin of cancer cell energy metabolism and of yeast glucose repression. *Biochimica et Biophysica Acta (BBA) - Bioenergetics* **1807**:568-576 https://doi.org/10.1016/j.bbabio.2010.08.010 | PubMed

14. **Dixon AS,** Schwinn MK, Hall MP, Zimmerman K, Otto P, Lubben TH, Butler BL, Binkowski BF, Machleidt T, Kirkland TA, *et al.* (2016) NanoLuc Complementation Reporter Optimized for Accurate Measurement of Protein Interactions in Cells. *ACS Chemical Biology* **11**:400-408 https://doi.org/10.1021/acschembio.5b00753 | PubMed

15. **Eto K,** Tsubamoto Y, Terauchi Y, Sugiyama T, Kishimoto T, Takahashi N, Yamauchi N, Kubota N, Murayama S, Aizawa T, *et al.* (1999) Role of NADH Shuttle System in Glucose-Induced Activation of Mitochondrial Metabolism and Insulin Secretion. *Science* **283**:981-985 https://doi.org/10.1126/science.283.5404.981 | PubMed

16. **Fukuda J,** Tsujimura S, Kano K (2008) Coulometric bioelectrocatalytic reactions based on NAD-dependent dehydrogenases in tricarboxylic acid cycle. *Electrochimica Acta* **54**:328-333 https://doi.org/10.1016/J.ELECTACTA.2008.07.071

17. **Gancedo JM** (1998) Yeast Carbon Catabolite Repression. *Microbiology and Molecular Biology Reviews* **62**:334-361 https://doi.org/10.1128/MMBR.62.2.334-361.1998 | PubMed

18. **Gerstmeir R,** Wendisch VF, Schnicke S, Ruan H, Farwick M, Reinscheid D, Eikmanns BJ (2003) Acetate metabolism and its regulation in Corynebacterium glutamicum. *Journal of Biotechnology* **104**:99-122 https://doi.org/10.1016/S0168-1656(03)00167-6 | PubMed

19. **Guaragnella N,** Ždralević M, Lattanzio P, Marzulli D, Pracheil T, Liu Z, Passarella S, Marra E, Giannattasio S. (2013) Yeast growth in raffinose results in resistance to acetic-acid induced programmed cell death mostly due to the activation of the mitochondrial retrograde pathway. *Biochimica et Biophysica Acta (BBA) - Molecular Cell Research* **1833**:2765-2774 https://doi.org/10.1016/j.bbamcr.2013.07.017 | PubMed

20. **Halper LA,** Srere PA (1977) Interaction between citrate synthase and mitochondrial malate dehydrogenase in the presence of polyethylene glycol. *Archives of biochemistry and biophysics* **184**:529-534 PubMed | https://doi.org/10.1016/0003-9861(77)90462-3

21. **Henriksen P,** Wagner SA, Weinert BT, Sharma S, Bačinskaja G, Rehman M, Juffer AH, Walther TC, Lisby M, Choudhary C (2012) Proteome-wide Analysis of Lysine Acetylation Suggests its Broad Regulatory Scope in Saccharomyces cerevisiae. *Molecular & Cellular Proteomics* **11**:1510-1522 https://doi.org/10.1074/mcp.M112.017251 | PubMed

22. **Herrgård MJ,** Swainston N, Dobson P, Dunn WB, Arga KY, Arvas M, Blüthgen N, Borger S, Costenoble R, Heinemann M, *et al.* (2008) A consensus yeast metabolic network reconstruction obtained from a community approach to systems biology. *Nature Biotechnology* **26**:1155-1160 https://doi.org/10.1038/nbt1492 | PubMed

23. **Holt LJ,** Tuch BB, Villén J, Johnson AD, Gygi SP, Morgan DO (2009) Global Analysis of Cdk1 Substrate Phosphorylation Sites Provides Insights into Evolution. *Science* **325**:1682-1686 https://doi.org/10.1126/science.1172867 | PubMed

24. **Hu C-D,** Chinenov Y, Kerppola TK (2002) Visualization of interactions among bZIP and Rel family proteins in living cells using bimolecular fluorescence complementation. *Molecular cell* **9**:789-98 PubMed | https://doi.org/10.1016/s1097-2765(02)00496-3

25. **Huang YM,** Huber GA, Wang N, Minteer SD, Mccammon JA (2018) Brownian dynamic study of an enzyme metabolon in the TCA cycle: Substrate kinetics and channeling. *Protein Science* **27**:463-471 https://doi.org/10.1002/pro.3338 | PubMed

26. **Klein CJL,** Olsson L, Nielsen J (1998) Glucose control in Saccharomyces cerevisiae: the role of MIG1 in metabolic functions. *Microbiology* **144**:13-24 https://doi.org/10.1099/00221287-144-1-13 | PubMed

27. **Landgraf D,** Huh D, Hallacli E, Lindquist S (2016) Scarless Gene Tagging with One-Step Transformation and Two-Step Selection in Saccharomyces cerevisiae and Schizosaccharomyces pombe. *PLOS One* **11**:e0163950 https://doi.org/10.1371/journal.pone.0163950 | PubMed

28. **Lanz MC,** Yugandhar K, Gupta S, Sanford EJ, Faça VM, Vega S, Joiner AMN, Fromme JC, Yu H, Smolka MB (2021) In-depth and 3-dimensional exploration of the budding yeast phosphoproteome. *EMBO reports* **22** https://doi.org/10.15252/embr.202051121 | PubMed

29. **Lee YJ,** Jang JW, Kim KJ, Maeng PJ (2011) TCA cycle-independent acetate metabolism via the glyoxylate cycle in Saccharomyces cerevisiae. *Yeast* **28**:153-166 https://doi.org/10.1002/yea.1828 | PubMed

30. **Lehtinen S,** Marsellach FX, Codlin S, Schmidt A, Clément-Ziza M, Beyer A, Bähler J, Orengo C, Pancaldi V (2013) Stress induces remodelling of yeast interaction and co-expression networks. *Molecular BioSystems* **9**:1697-1707 https://doi.org/10.1039/C3MB25548D | PubMed

31. **Litsios A,** Ortega ÁD, Wit EC, Heinemann M (2018) Metabolic-flux dependent regulation of microbial physiology. *Current Opinion in Microbiology* **42**:71-78 https://doi.org/10.1016/j.mib.2017.10.029 | PubMed

32. **Liu Z,** Butow RA (2006) Mitochondrial Retrograde Signaling. *Annual Review of Genetics* **40**:159-185 https://doi.org/10.1146/annurev.genet.40.110405.090613 | PubMed

33. **Meyer FM,** Gerwig J, Hammer E, Herzberg C, Commichau FM, Völker U, Stülke J (2011) Physical interactions between tricarboxylic acid cycle enzymes in Bacillus subtilis: Evidence for a metabolon. *Metabolic Engineering* **13**:18-27 https://doi.org/10.1016/j.ymben.2010.10.001 | PubMed

34. **Molinié T,** Cougouilles E, David C, Cahoreau E, Portais J-C, Mourier A (2022) MDH2 produced OAA is a metabolic switch rewiring the fuelling of respiratory chain and TCA cycle. *Biochimica et Biophysica Acta (BBA) - Bioenergetics* **1863**:148532 https://doi.org/10.1016/j.bbabio.2022.148532 | PubMed

35. **Morgan B,** Sobotta MC, Dick TP (2011) Measuring EGSH and H2O2 with roGFP2-based redox probes. *Free Radical Biology and Medicine* **51**:1943-1951 https://doi.org/10.1016/j.freeradbiomed.2011.08.035 | PubMed

36. **Morgunov I,** Srere PA (1998) Interaction between citrate synthase and malate dehydrogenase: Substrate channeling of oxaloacetate. *Journal of Biological Chemistry* **273**:29540-29544 https://doi.org/10.1074/jbc.273.45.29540 | PubMed

37. **Mukherjee M,** Nandi A, Chandra K, Saikia SK, Jana CK, Das N (2020) Protein extraction from Saccharomyces cerevisiae at different growth phases. *Journal of Microbiological Methods* **172**:105906 https://doi.org/10.1016/j.mimet.2020.105906 | PubMed

38. **Noor E,** Bar-Even A, Flamholz A, Reznik E, Liebermeister W, Milo R (2014) Pathway thermodynamics highlights kinetic obstacles in central metabolism. *PLoS computational biology* **10**:e1003483 https://doi.org/10.1371/journal.pcbi.1003483 | PubMed

39. **Obata T** (2020) Toward an evaluation of metabolite channeling in vivo. *Current Opinion in Biotechnology* **64**:55-61 https://doi.org/10.1016/j.copbio.2019.09.013 | PubMed

40. **Obata T** (2019) Metabolons in plant primary and secondary metabolism. *Phytochemistry Reviews* **18**:1483-1507 https://doi.org/10.1007/s11101-019-09619-x

41. **Obata T,** Schoenefeld S, Krahnert I, Bergmann S, Scheffel A, Fernie A (2013) Gas-Chromatography Mass-Spectrometry (GC-MS) Based Metabolite Profiling Reveals Mannitol as a Major Storage Carbohydrate in the Coccolithophorid Alga Emiliania huxleyi. *Metabolites* **3**:168-184 https://doi.org/10.3390/metabo3010168 | PubMed

42. **Omini J.** (2024) Doctoral dissertation: Role of the Malate Dehydrogenase-Citrate Synthase Metabolon in Metabolic Flux Regulation. University of Nebraska-Lincoln.

43. **Omini J,** Dele-Osibanjo T, Kim H, Zhang J, Obata T (2024) Is the TCA cycle malate dehydrogenase-citrate synthase metabolon an illusion?. *Essays in Biochemistry* https://doi.org/10.1042/EBC20230084 | PubMed

44. **Omini J,** Wojciechowska I, Skirycz A, Moriyama H, Obata T (2021) Association of the malate dehydrogenase-citrate synthase metabolon is modulated by intermediates of the Krebs tricarboxylic acid cycle. *Scientific Reports* **11**:18770 https://doi.org/10.1038/s41598-021-98314-z | PubMed

45. **Orij R,** Postmus J, Ter Beek A, Brul S, Smits GJ (2009) In vivo measurement of cytosolic and mitochondrial pH using a pH-sensitive GFP derivative in Saccharomyces cerevisiae reveals a relation between intracellular pH and growth. *Microbiology* **155**:268-278 https://doi.org/10.1099/mic.0.022038-0 | PubMed

46. **Orlandi I,** Coppola D, Vai M (2014) Rewiring yeast acetate metabolism through MPC1 loss of function leads to mitochondrial damage and decreases chronological lifespan. *Microbial Cell* **1**:393-405 https://doi.org/10.15698/mic2014.12.178 | PubMed

47. **Pfeiffer T,** Morley A (2014) An evolutionary perspective on the Crabtree effect. *Frontiers in Molecular Biosciences* **1** https://doi.org/10.3389/fmolb.2014.00017 | PubMed

48. **Polakis E,** Bartley W (1965) Changes in the enzyme activities of Saccharomyces cerevisiae during aerobic growth on different carbon sources. *Biochemical Journal* **97**:284-297 https://doi.org/10.1042/bj0970284 | PubMed

49. **Rajasekaran S,** Peterson PP, Liu Z, Robinson LC, Witt SN (2022) α-synuclein inhibits Snx3-retromer retrograde trafficking of the conserved membrane-bound proprotein convertase Kex2 in the secretory pathway of Saccharomyces cerevisiae. *Human Molecular Genetics* **31**:705-717 https://doi.org/10.1093/hmg/ddab284 | PubMed

50. **Reinders J,** Wagner K, Zahedi RP, Stojanovski D, Eyrich B, van der Laan M, Rehling P, Sickmann A, Pfanner N, Meisinger C. (2007) Profiling Phosphoproteins of Yeast Mitochondria Reveals a Role of Phosphorylation in Assembly of the ATP Synthase. *Molecular & Cellular Proteomics* **6**:1896-1906 https://doi.org/10.1074/mcp.M700098-MCP200 | PubMed

51. **Rep M,** Reiser V, Gartner U, Thevelein JM, Hohmann S, Ammerer G, Ruis H (1999) Osmotic Stress-Induced Gene Expression in Saccharomyces cerevisiae Requires Msn1p and the Novel Nuclear Factor Hot1p. *Molecular and Cellular Biology* **19**:5474-5485 https://doi.org/10.1128/MCB.19.8.5474 | PubMed

52. **Robinson JB,** Inman L, Sumegi B, Srere PA (1987) Further characterization of the Krebs tricarboxylic acid cycle metabolon. *The Journal of biological chemistry* **262**:1786-1790 PubMed | https://doi.org/10.1016/s0021-9258(19)75707-x

53. **Rogers S,** Hariri H, Wood NE, Speer NO, Henne WM (2021) Glucose restriction drives spatial reorganization of mevalonate metabolism. *eLife* **10**:e62591 https://doi.org/10.7554/eLife.62591 | PubMed

54. **Rolland F,** Winderickx J, Thevelein JM (2002) Glucose-sensing and -signalling mechanisms in yeast. *FEMS Yeast Research* **2**:183-201 https://doi.org/10.1111/j.1567-1364.2002.tb00084.x | PubMed

55. **Ronne H** (1995) Glucose repression in fungi. *Trends in Genetics* **11**:12-17 https://doi.org/10.1016/S0168-9525(00)88980-5 | PubMed

56. **Rosado CJ,** Mijaljica D, Hatzinisiriou I, Prescott M, Devenish RJ (2008) Rosella: A fluorescent pH-biosensor for reporting vacuolar turnover of cytosol and organelles in yeast. *Autophagy* **4**:205-213 https://doi.org/10.4161/auto.5331 | PubMed

57. **Santo-Domingo J,** Demaurex N (2012) The renaissance of mitochondrial pH. *Journal of General Physiology* **139**:415-423 https://doi.org/10.1085/jgp.201110767 | PubMed

58. **Sarrion-Perdigones A,** Vazquez-Vilar M, Palaci J, Castelijns B, Forment J, Ziarsolo P, Blanca J, Granell A, Orzaez D (2013) GoldenBraid 2.0: A Comprehensive DNA Assembly Framework for Plant Synthetic Biology. *Plant Physiology* **162**:1618-1631 https://doi.org/10.1104/pp.113.217661 | PubMed

59. **Schüller H-J** (2003) Transcriptional control of nonfermentative metabolism in the yeast Saccharomyces cerevisiae. *Current Genetics* **43**:139-160 https://doi.org/10.1007/s00294-003-0381-8 | PubMed

60. **Selivanov VA,** Zeak JA, Roca J, Cascante M, Trucco M, Votyakova T V (2008) The Role of External and Matrix pH in Mitochondrial Reactive Oxygen Species Generation. *Journal of Biological Chemistry* **283**:29292-29300 https://doi.org/10.1074/jbc.M801019200 | PubMed

61. **Spivey HO,** Ovádi J (1999) Substrate channeling. *Methods* **19**:306-321 https://doi.org/10.1006/meth.1999.0858 | PubMed

62. **Srere PA** (1985) The metabolon. *Trends in Biochemical Sciences* **10**:109-110 https://doi.org/10.1016/0968-0004(85)90266-X

63. **Srere PA** (1969) [1] Citrate synthase. *Methods in Enzymology* 3-11 https://doi.org/10.1016/0076-6879(69)13005-0

64. **Strittmatter CF** (1957) Adaptive Variation in the Level of Oxidative Activity in Saccharomyces cerevisiae. *Journal of General Microbiology* **16**:169-183 https://doi.org/10.1099/00221287-16-1-169

65. **Sumegi B,** Sherry AD, Malloy CR, Srere PA (1993) Evidence for orientation-conserved transfer in the TCA cycle in Saccharomyces cerevisiae: carbon-13 NMR studies. *Biochemistry* **32**:12725-12729 https://doi.org/10.1021/bi00210a022 | PubMed

66. **Swaney DL,** Beltrao P, Starita L, Guo A, Rush J, Fields S, Krogan NJ, Villén J (2013) Global analysis of phosphorylation and ubiquitylation cross-talk in protein degradation. *Nature Methods* **10**:676-682 https://doi.org/10.1038/nmeth.2519 | PubMed

67. **Sweetlove LJ,** Beard KFM, Nunes-Nesi A, Fernie AR, Ratcliffe RG (2010) Not just a circle: Flux modes in the plant TCA cycle. *Trends in Plant Science* **15**:462-470 https://doi.org/10.1016/j.tplants.2010.05.006 | PubMed

68. **Thierie J,** Penninckx M (2010) Crabtree Effect. *Encyclopedia of Industrial Biotechnology* https://doi.org/10.1002/9780470054581.eib243

69. **Tompa P,** Batke J, Ovadi J, Welch GR, Srere PA (1987) Quantitation of the interaction between citrate synthase and malate dehydrogenase. *Journal of Biological Chemistry* **262**:6089-6092 https://doi.org/10.1016/S0021-9258(18)45541-X

70. **van Urk H,** Schipper D, Breedveld GJ, Mak PR, Alexander Scheffers W, van Dijken JP (1989) Localization and kinetics of pyruvate-metabolizing enzymes in relation to aerobic alcoholic fermentation in Saccharomyces cerevisiae CBS 8066 and Candida utilis CBS 621. *Biochimica et Biophysica Acta (BBA)* -

General Subjects **992**:78-86 https://doi.org/10.1016/0304-4165(89)90053-6 | PubMed

71. **Vevea JD,** Alessi Wolken DM, Swayne TC, White AB, Pon LA (2013) Ratiometric Biosensors that Measure Mitochondrial Redox State and ATP in Living Yeast Cells. *Journal of Visualized Experiments* 1-12 https://doi.org/10.3791/50633 | PubMed

72. **Vilela-Moura A,** Schuller D, Mendes-Faia A, Silva RD, Chaves SR, Sousa MJ, Côrte-Real M (2011) The impact of acetate metabolism on yeast fermentative performance and wine quality: reduction of volatile acidity of grape musts and wines. *Applied Microbiology and Biotechnology* **89**:271-280 https://doi.org/10.1007/s00253-010-2898-3 | PubMed

73. **Wase N,** Abshire N, Obata T (2022) High-Throughput Profiling of Metabolic Phenotypes Using High-Resolution GC-MS. *Methods in molecular biology* 235-260 https://doi.org/10.1007/978-1-0716-2537-8_19 | PubMed

74. **Weinert BT,** Schölz C, Wagner SA, Iesmantavicius V, Su D, Daniel JA, Choudhary C (2013) Lysine Succinylation Is a Frequently Occurring Modification in Prokaryotes and Eukaryotes and Extensively Overlaps with Acetylation. *Cell Reports* **4**:842-851 https://doi.org/10.1016/j.celrep.2013.07.024 | PubMed

75. **Wheeldon I,** Minteer SD, Banta S, Barton SC, Atanassov P, Sigman M (2016) Substrate channelling as an approach to cascade reactions. *Nature Chemistry* **8**:299-309 https://doi.org/10.1038/nchem.2459 | PubMed

76. **Williamson JR,** Cooper RH (1980) Regulation of the citric acid cycle in mammalian systems. *FEBS Letters* **117**:K73-K85 https://doi.org/10.1016/0014-5793(80)80572-2 | PubMed

77. **Wu F,** Minteer S (2015) Krebs Cycle Metabolon: Structural Evidence of Substrate Channeling Revealed by Cross-Linking and Mass Spectrometry. *Angewandte Chemie International Edition* **54**:1851-1854 https://doi.org/10.1002/anie.201409336 | PubMed

78. **Wu F,** Pelster LN, Minteer SD (2015) Krebs cycle metabolon formation: metabolite concentration gradient enhanced compartmentation of sequential enzymes. *Chemical Communications* **51**:1244-1247 https://doi.org/10.1039/C4CC08702J | PubMed

79. **Yin X,** Li J, Shin H, Du G, Liu L, Chen J (2015) Metabolic engineering in the biotechnological production of organic acids in the tricarboxylic acid cycle of microorganisms: Advances and prospects. *Biotechnology Advances* **33**:830-841 https://doi.org/10.1016/j.biotechadv.2015.04.006 | PubMed

80. **Zhang T,** Lei J, Yang H, Xu K, Wang R, Zhang Z (2011) An improved method for whole protein extraction from yeast Saccharomyces cerevisiae. *Yeast* **28**:795-798 https://doi.org/10.1002/yea.1905 | PubMed

81. **Zhang Y,** Beard KFM, Swart C, Bergmann S, Krahnert I, Nikoloski Z, Graf A, Ratcliffe RG, Sweetlove LJ, Fernie AR, *et al.* (2017) Protein-protein interactions and metabolite channelling in the plant tricarboxylic acid cycle. *Nature communications* **8**:15212 https://doi.org/10.1038/ncomms15212 | PubMed

82. **Zhang Y,** Su M, Wang Z, Nielsen J, Liu Z (2022) Rewiring regulation on respiro-fermentative metabolism relieved Crabtree effects in Saccharomyces cerevisiae. *Synthetic and Systems Biotechnology* **7**:1034-1043 https://doi.org/10.1016/j.synbio.2022.06.004 | PubMed

83. **Zhu Y,** Jin L, Shi R, Li J, Wang Y, Zhang L, Liang C-Z, Narayana VK, De Souza DP, Thorne RF, *et al.* (2022) The long noncoding RNA glycoLINC assembles a lower glycolytic metabolon to promote glycolysis. *Molecular Cell* **82**:542-554.e6. https://doi.org/10.1016/j.molcel.2021.11.017 | PubMed

Peer reviews

Reviewer #1 (Public review):

Summary:

The study by the Obata group characterizes the dynamics of the canonical malate dehydrogenase-citrate synthase metabolon in yeast.

Strengths:

The study is well-written and appears to give clear demonstrations of this phenomenon.

Studies of the dynamics of metabolon formation are rare; if the authors can address the concern detailed below, then they have provided such for one of the canonical metabolons in nature.

Weaknesses:

There is a fundamental issue with the study, which is that the authors do not provide enough support or information concerning the split luciferase system that they use. Is the binding reversible or not? How the data is interpreted is massively influenced by this fact. What are the pros and cons of this method in comparison to, for example, FLIM-FRET? The authors state that the method is semi-quantitative - can they document this? All of the conclusions are based on the quality of this method. I know that it has been used by others, but at least some preliminary documentation to address these questions is required.

Comments on revised version:

I feel that the authors have adequately addressed my prior concerns. I have no further critiques of their work.

https://doi.org/10.7554/eLife.107953.2.sa3

Reviewer #2 (Public review):

This study explores the dynamic association between malate dehydrogenase (MDH1) and citrate synthase (CIT1) in Saccharomyces cerevisiae, with the aim of linking this interaction to respiratory metabolism. Utilizing a NanoBiT split-luciferase system, the authors monitor protein-protein interactions in vivo under various metabolic conditions.

Major Concerns:

(1) NanoBiT Signal May Reflect Protein Abundance Rather Than Interaction Strength

In Figure 1C, the authors report increased MDH1-CIT1 interaction under respiratory (acetate) conditions and decreased interaction during fermentation (glucose), as indicated by NanoBiT luminescence. However, this signal appears to correlate strongly with the expression levels of MDH1 and CIT1, raising the possibility that the observed luminescence reflects protein abundance rather than specific interaction dynamics. To resolve this, NanoBiT signals should be normalized to the expression levels of both proteins to distinguish between abundance-driven and interaction-driven changes.

(2) Lack of Causal Evidence

The study presents a series of metabolic perturbation experiments (e.g., arsenite, AOA, antimycin A, malonate) and correlates changes in metabolite levels with NanoBiT signals. However, these data are correlative and do not establish a functional role for the MDH1-CIT1 interaction in metabolic regulation. To demonstrate causality, the authors should implement approaches to specifically disrupt the MDH1-CIT1 interaction. One strategy could involve using a 15-residue peptide (Pept1) derived from the Pro354-Pro366 region of CIT1, previously shown to mediate the interaction or introducing the cit1Δ3 (Arg362Glu) mutation, which perturbs binding. Metabolic flux analysis using ^13C-labeled glucose and mitochondrial respiration assays (e.g., Seahorse) could then assess functional consequences.

(3) Absence of Protein Expression Controls Under Perturbation Conditions

In experiments involving acetate, arsenite, AOA, antimycin A, and malonate, the authors infer changes in MDH1-CIT1 association based solely on NanoBiT signals. However, no accompanying data are provided on MDH1 and CIT1 protein levels under these conditions. This omission weakens the conclusions, as altered expression rather than interaction strength could underlie the observed luminescence changes. Immunoblotting or quantitative proteomics should be used to confirm constant protein expression across conditions.

Conclusion:

Although the central question is compelling and the use of NanoBiT in live cells is a strength, the manuscript requires additional experimental rigor. Specifically, normalization of interaction signals, introduction of causative perturbations, and validation of protein expression are essential to substantiate the study's claims.

Comments on revised version:

The manuscript is much improved.

https://doi.org/10.7554/eLife.107953.2.sa2

Reviewer #3 (Public review):

Summary:

Metabolons are multisubunit complexes that promote the physical association of sequential enzymes within a metabolic pathway. Such complexes are proposed to increase metabolic flux and efficiency by channeling reaction intermediates between enzymes. The TCA cycle enzymes malate dehydrogenase (MDH1) and citrate synthase (CIT1) have been linked to metabolon formation, yet the conditions under which these enzymes interact, and whether such interactions are dynamic in response to metabolic cues, remains unclear, particularly in the native cellular context. This study uses a nanoBIT protein-protein interaction assay to map the dynamic behavior of the MDH1-CIT1 interaction in response to multiple metabolic stimuli and challenges in yeast. Beyond mapping these interactions in real time, the authors also performed GC-MS metabolomics to map whole cell metabolite alterations across experimental conditions. Finally, the authors use microscale thermophoresis to determine components that alter the MDH1-CIT1 interaction in vitro. Collectively, the authors synthesize their collected data into a model in which the MDH1-CIT1 metabolon dissociates in conditions of low respiratory flux, and is stimulated during conditions of high respiratory flux. While their data largely support these models, some key exceptions are found that suggest this model is likely oversimplified and will require further work to understand the complexities associated with MDH1-CIT1 interaction dynamics. Nonetheless, the authors put forth an interesting and timely toolkit to begin to understand the interaction kinetics and dynamics of key metabolic enzymes that should serve as a platform to begin disentangling these important yet understudied aspects of metabolic regulation.

Strengths:

- The authors address an important question: how do metabolon-associated protein protein interactions change across altered metabolic conditions?

- The development and validation of the MDH1-CIT1 nanoBIT assay provides an important tool to allow the quantification of this protein-protein interaction in vivo. Importantly, the authors demonstrate that the assay allows kinetic and real time assessment of these protein interactions, which reveal interesting and dynamic behavior across conditions.

- The use of classic biochemical techniques to confirm that pH and various metabolites can alter the MDH1-CIT1 interaction in vitro is rigorous and supports the model put forth by the

authors.

Weaknesses:

The authors have addressed identified weaknesses within the revision of their manuscript.

https://doi.org/10.7554/eLife.107953.2.sa1

Author response:

The following is the authors' response to the original reviews.

> ***eLife Assessment***
>
> *This study reports a dynamic association/dissociation between malate dehydrogenase (MDH1) and citrate synthase (CIT1) in Saccharomyces cerevisiae under different metabolic conditions that control TCA pathway flux rate. The research question is timely, the use of the NanoBiT split-luciferase system to monitor protein-protein interactions is innovative, and the significance of the findings is valuable. However, the strength of evidence needed to support the conclusions was found to be incomplete based on a lack of critical control and mechanistic experiments.*

We thank the editor for this thoughtful assessment of our work. We are encouraged that the research question, experimental approach, and overall significance were viewed positively.

To address the concern regarding the strength of evidence, we have implemented additional controls in the revised manuscript. Specifically, we have repeated all MDH1CIT1 interaction measurements alongside strains expressing full-length NanoLUC fusion proteins to assess MDH1 and CIT1 protein abundance. The resulting data, now included as supplementary figures (Figure 2 – figure supplement 2, Figure 2 – figure supplement 3, Figure 3 – figure supplement 1, Figure 4 – figure supplement 2), demonstrate the reproducibility of the findings and indicate that the observed changes in MDH1-CIT1 interaction are not attributable to protein abundance variations.

We agree that a detailed mechanistic dissection of how the MDH1–CIT1 complex influences metabolic pathway flux is an essential piece of evidence for establishing the functions of the metabolon. However, such analyses require extensive additional investigation beyond the scope of the present study. Accordingly, we have clarified the aims of this work in the revised manuscript to emphasize that our primary objective is to characterize the dynamic behavior of the MDH1–CIT1 interaction under different metabolic conditions and to identify key factors associated with its regulation.

We believe these revisions strengthen the rigor of the study, better define its scope, and provide a solid foundation for future mechanistic investigations.

> ***Public Reviews:***
>
> ***Reviewer #1 (Public review):***
>
> *Summary:*
>
> *The study by the Obata group characterizes the dynamics of the canonical malate dehydrogenase-citrate synthase metabolon in yeast.*
>
> *Strengths:*
>
> *The study is well-written and appears to give clear demonstrations of this phenomenon.*

> *Studies of the dynamics of metabolon formation are rare; if the authors can address the concern detailed below, then they have provided such for one of the canonical metabolons in nature.*

We sincerely thank the reviewer for their positive assessment and for recognizing the value of our study in characterizing the dynamics of the MDH1-CIT1 metabolon. We appreciate the recognition that studies of metabolon dynamics are rare and that our work provides a clear demonstration of this phenomenon for a canonical metabolon. We have carefully addressed the methodological concerns regarding the NanoBiT system as detailed below to further strengthen the evidence for our findings.

> *Weaknesses:*
>
> *There is a fundamental issue with the study, which is that the authors do not provide enough support or information concerning the split luciferase system that they use.*

We agree that a detailed description of the NanoBiT system is essential to ensure the reliability of the methodology. As suggested, we have added a dedicated paragraph to the Introduction (Lines 90–103) to clarify these technical aspects, supported by the foundational work of Dixon et al. (2016).

> *Is the binding reversible or not? How the data is interpreted is massively influenced by this fact.*

Yes, the NanoBiT system is specifically designed to be reversible. The intrinsic affinity of the subunits is low (K_D = 190 µM), and the association and dissociation rate constants (k_{on} = 500 $M^{-1}s^{-1}$, k_{off} = 0.2 s^{-1}) are well outside the range of typical protein-protein interactions (Dixon et al., 2016). These kinetics ensure that the assembly and disassembly of the luminescent complex are dictated solely by the interaction characteristics of the target proteins (MDH1 and CIT1) and not by the tags themselves. This allows for real-time monitoring of both the association and dissociation phases.

> *What are the pros and cons of this method in comparison to, for example, FLIM-FRET?*

We have now explicitly addressed the pros and cons of our methodology compared to fluorescence-based systems:

Pros: The NanoLUC-based reporter is 150 times brighter than conventional luciferases and has a significantly higher dynamic range (Hall et al 2016), allowing detection of weak transient interactions. Importantly for this study, fluorescence-based methods such as FLIM-FRET and BRET are difficult to implement in yeast microplate assays due to the high levels of cellular autofluorescence. NanoBiT bypasses this issue, providing a high signal-tonoise ratio.

Cons: Unlike FRET, NanoBiT requires the application of a substrate (furimazine). We did not include this disadvantage in the manuscript because it is not critical in a yeast study. Furimazine can be applied directly to the medium and readily permeates cells.

> *The authors state that the method is semi-quantitative - can they document this?*

The semi-quantitative nature of the system is supported by its high dynamic range and the linear relationship between the luminescence signal and the amount of protein complex formed, as documented in Dixon et al. (2016). By using this system in a microplate setting, we were able to monitor relative increases or decreases in interaction levels over time across multiple metabolic conditions, providing a robust comparative analysis of metabolon dynamics.

> *All of the conclusions are based on the quality of this method. I know that it has been used by others, but at least some preliminary documentation to address these questions is required.*

We acknowledge the reviewer's concern regarding the reliance on the NanoBiT system. To ensure the reliability of our conclusions, we have included several lines of evidence to validate the method and demonstrate that the observed luminescence signals accurately reflect protein-protein interaction dynamics.

To confirm the NanoBiT results using an independent biochemical approach, we performed an *in vivo* pull-down assay following glucose addition (Figure 2 – figure supplement 1A). The results demonstrate a reduction in the physical association between MDH1 and CIT1. This biochemical validation directly supports the reduction in interaction observed with the NanoBiT system during the Crabtree effect.

We have provided protein abundance data for both MDH1 and CIT1 across the experimental conditions (Figure 2 – figure supplement 1&3; Figure 3 – figure supplement 1; Figure 4 – figure supplement 2). These results show only minor changes in protein levels, confirming that the fluctuations in the NanoBiT signal are independent of protein expression and represent genuine changes in metabolon assembly.

To ensure the findings are reproducible, we have included MDH1-CIT1 interaction results from repeated independent experiments (Figure 2 – figure supplement 1&3; Figure 3 – figure supplement 1; Figure 4 – figure supplement 1). The consistency of the results across these trials confirms the robustness of the system in monitoring the metabolic regulation of this complex.

We hope that these additional experimental validations, alongside the detailed technical description based on the established properties of the NanoBiT system (Dixon et al., 2016; Hall et al., 2012), provide the necessary documentation to satisfy the reviewer's concerns regarding the quality and reliability of the method.

> ***Reviewer #2 (Public review):***
>
> *This study explores the dynamic association between malate dehydrogenase (MDH1) and citrate synthase (CIT1) in Saccharomyces cerevisiae, with the aim of linking this interaction to respiratory metabolism. Utilizing a NanoBiT split-luciferase system, the authors monitor protein-protein interactions in vivo under various metabolic conditions.*
>
> *Major Concerns:*
>
> *(1) NanoBiT Signal May Reflect Protein Abundance Rather Than Interaction Strength*
>
> *In Figure 1C, the authors report increased MDH1-CIT1 interaction under respiratory (acetate) conditions and decreased interaction during fermentation (glucose), as indicated by NanoBiT luminescence. However, this signal appears to correlate strongly with the expression levels of MDH1 and CIT1, raising the possibility that the observed luminescence reflects protein abundance rather than specific interaction dynamics. To resolve this, NanoBiT signals should be normalized to the expression levels of both proteins to distinguish between abundance-driven and interaction-driven changes.*

We agree that distinguishing between abundance-driven and interaction-driven changes is vital. To address this, we have included new data showing the relative protein levels of MDH1 and CIT1 across all experimental conditions. The protein levels were assessed using yeast lines expressing these proteins tagged with full-length NanoLUC luciferase (Figure 2 – figure supplement 1&3, Figure 3 - figure supplement 1, Figure 4 – figure supplement 2). Using the luminescence data of these relative protein levels, we have included plots showing

normalized interaction index (Figure 2 – figure supplement 1G & 3D,H,L; Figure 3 - figure supplement 1D,H,L P; Figure 4 – figure supplement 1D,H,L). This index was calculated by dividing the NanoBiT interaction signal by the product of the relative abundances of both proteins:

$$\text{Normalized Interaction Index} = \frac{\text{NanoBit}}{\text{MDH 1} * \text{CIT 1}}$$

In this formula, NanoBiT, MDH1, and CIT1 are the relative luminescence levels at each time point. This analysis clarified that the changes in the interaction signal significantly exceeded the fluctuations in protein levels, confirming that the dynamics are interactionspecific and not abundance-driven. To provide the most direct and transparent representation of the experimental measurements, we have chosen to keep the raw RLU data in the main figures and have moved the data related to protein abundance and normalization to figure supplements.

> *(2) Lack of Causal Evidence*
>
> *The study presents a series of metabolic perturbation experiments (e.g., arsenite, AOA, antimycin A, malonate) and correlates changes in metabolite levels with NanoBiT signals. However, these data are correlative and do not establish a functional role for the MDH1CIT1 interaction in metabolic regulation. To demonstrate causality, the authors should implement approaches to specifically disrupt the MDH1-CIT1 interaction. One strategy could involve using a 15-residue peptide (Pept1) derived from the Pro354-Pro366 region of CIT1, previously shown to mediate the interaction, or introducing the cit1Δ3 (Arg362Glu) mutation, which perturbs binding. Metabolic flux analysis using ^13C-labeled glucose and mitochondrial respiration assays (e.g., Seahorse) could then assess functional consequences.*

We agree with the reviewer that the current dataset correlates metabolon assembly with metabolic states rather than establishing a direct causal proof of its functional role in regulating pathway flux.

However, the primary objective of this manuscript was to establish the dynamic nature of the MDH1-CIT1 metabolon and to demonstrate the causal relationship between the changes in cellular conditions and metabolon dynamics through *in vitro* and *in vivo* assessments. Demonstrating that this canonical multienzyme complex undergoes reversible assembly and disassembly in vivo represents a major advance, as metabolon dynamics is a critical, yet previously unrevealed, factor involved in metabolic regulation. We aimed to define the specific environmental triggers that govern these dynamics, providing the necessary foundation for defining the functions of metabolons.

We completely agree that establishing causality using interaction-deficient mutants coupled with metabolic flux analysis is another critical experiment to establish the functions of the TCA cycle metabolon. We have, in fact, been conducting these precise metabolic flux analyses on CIT1 mutants with disrupted interaction with MDH1. Because the functional consequences of complex disruption involve wide-reaching metabolic rerouting that requires extensive data presentation and modeling, this work forms a separate, comprehensive follow-up study that is currently in preparation for submission in the near future.

To address this limitation in the current manuscript, we have carefully reviewed and revised the Abstract, Results, Discussion, and Conclusion sections (Lines 19-22; 205; 322-327; 341-342; 458-466). We have removed any language that may have inadvertently implied direct causality. We now explicitly state that our findings indicate the relationship between metabolon dynamics and respiratory conditions, and we have added a clear statement noting that the direct effects of this assembly on metabolic flux are the focus of our forthcoming studies.

> *(3) Absence of Protein Expression Controls Under Perturbation Conditions*
>
> *In experiments involving acetate, arsenite, AOA, antimycin A, and malonate, the authors infer changes in MDH1-CIT1 association based solely on NanoBiT signals. However, no accompanying data are provided on MDH1 and CIT1 protein levels under these conditions. This omission weakens the conclusions, as altered expression rather than interaction strength could underlie the observed luminescence changes. Immunoblotting or quantitative proteomics should be used to confirm constant protein expression across conditions.*

In response to your first concern, we have now performed protein expression assessments for all experiments, including the perturbation conditions, such as acetate, arsenite, AOA (Figure 3 – figure supplement 1), antimycin A, cyanide, and malonate (Figure 4 – figure supplement 2). The results demonstrate that the protein levels of MDH1 and CIT1 remain relatively stable throughout these treatments and do not correlate with the large changes observed in the interaction signals. This is also demonstrated by the normalized interaction index, which confirms that the shifts in luminescence are driven by the dynamic assembly and disassembly of the MDH1-CIT1 metabolon rather than changes in protein concentrations.

> *Conclusion:*
>
> *Although the central question is compelling and the use of NanoBiT in live cells is a strength, the manuscript requires additional experimental rigor. Specifically, normalization of interaction signals, introduction of causative perturbations, and validation of protein expression are essential to substantiate the study's claims.*

We sincerely thank the reviewer for recognizing the value of our central question and the strength of the live-cell NanoBiT system, as well as for your rigorous critique that has strengthened this manuscript. To address the concerns regarding experimental rigor, we have now provided extensive validation of MDH1 and CIT1 protein expression across all experimental conditions using yeast lines tagged with the full-length NanoLUC luciferase. These data demonstrate relatively stable protein expression, allowing us to calculate a normalized interaction index that substantiates that the observed luminescence shifts are driven by dynamic metabolon assembly rather than protein concentration. Regarding causative perturbations, we agree that introducing interaction-deficient mutants coupled with isotopic flux analysis is the critical next step to establish functional consequences. Because defining these pathway-wide rerouting events requires extensive modeling, this work will be reported in a follow-up study currently in preparation. Accordingly, we have carefully revised the manuscript to remove language implying direct causality, explicitly framing metabolon dynamics as an integral factor in metabolic regulation closely related to pathway activity and cellular metabolic states. We believe these new quantitative controls, normalizations, and textual clarifications thoroughly address the need for additional rigor and solidly substantiate our findings.

> ***Reviewer #3 (Public review):***
>
> *Summary:*
>
> *Metabolons are multisubunit complexes that promote the physical association of sequential enzymes within a metabolic pathway. Such complexes are proposed to increase metabolic flux and efficiency by channeling reaction intermediates between enzymes. The TCA cycle enzymes malate dehydrogenase (MDH1) and citrate synthase (CIT1) have been linked to metabolon formation, yet the conditions under which these enzymes interact, and whether such interactions are dynamic in response to metabolic cues, remain unclear, particularly in the native cellular context. This study uses a nanoBIT protein-protein interaction assay to map the dynamic behavior of the MDH1-*

> *CIT1 interaction in response to multiple metabolic stimuli and challenges in yeast. Beyond mapping these interactions in real time, the authors also performed GC-MS metabolomics to map whole-cell metabolite alterations across experimental conditions. Finally, the authors use microscale thermophoresis to determine components that alter the MDH1-CIT1 interaction in vitro. Collectively, the authors synthesize their collected data into a model in which the MDH1CIT1 metabolon dissociates in conditions of low respiratory flux, and is stimulated during conditions of high respiratory flux. While their data largely support these models, some key exceptions are found that suggest this model is likely oversimplified and will require further work to understand the complexities associated with MDH1-CIT1 interaction dynamics. Nonetheless, the authors put forth an interesting and timely toolkit to begin to understand the interaction kinetics and dynamics of key metabolic enzymes that should serve as a platform to begin disentangling these important yet understudied aspects of metabolic regulation.*

We thank the reviewer for this thoughtful and constructive summary of our work. We appreciate the recognition of the novelty and utility of our experimental approach and the integrated analysis of MDH1–CIT1 interaction dynamics.

We agree with the reviewer that, although our data largely support a model in which MDH1–CIT1 interaction correlates with respiratory activity, there are conditions that do not fully conform to this simplified framework. In the revised manuscript, we have addressed these apparent inconsistencies by providing detailed interpretations of the counterintuitive observations (e.g., ETC inhibition) and emphasizing that the MDH1–CIT1 interaction is modulated by changes in the mitochondrial matrix microenvironment associated with respiratory activity.

Furthermore, we have revised the Discussion to highlight that the regulation of the MDH1–CIT1 interaction is likely multifactorial, involving the combined effects of pH, metabolites, and other unknown factors, which together enable fine-tuning of metabolic flux in fluctuating environments. This expanded perspective is now more clarified.

We agree that identifying the precise molecular determinants of MDH1–CIT1 interaction dynamics will require additional mechanistic studies, such as systematic analyses using yeast mutants. While these experiments are an important next step, they are beyond the scope of the present study. We anticipate that the toolkit and framework established here will facilitate such future investigations.

> *Strengths:*
>
> *(1) The authors address an important question: how do metabolon-associated proteinprotein interactions change across altered metabolic conditions?*
>
> *(2) The development and validation of the MDH1-CIT1 nanoBIT assay provides an important tool to allow the quantification of this protein-protein interaction in vivo. Importantly, the authors demonstrate that the assay allows kinetic and real time assessment of these protein interactions, which reveal interesting and dynamic behavior across conditions.*
>
> *(3) The use of classic biochemical techniques to confirm that pH and various metabolites can alter the MDH1-CIT1 interaction in vitro is rigorous and supports the model put forth by the authors.*

We thank the reviewer for these positive and encouraging comments. We are pleased that the importance of the research question, the development of the MDH1–CIT1 NanoBiT assay, and the integration of in vivo and in vitro approaches were recognized. We especially appreciate the acknowledgment of the assay's ability to capture dynamic and kinetic changes in protein–protein interactions, as well as the support provided by the biochemical analyses. We hope

that the experimental framework established in this study will serve as a useful platform for further investigations into metabolon dynamics and metabolic regulation.

> *Weaknesses:*
>
> *(1) Some of the data collected seem to be merely reported rather than synthesized and interpreted for the reader.*

We agree that explicitly synthesizing these findings is essential for clarity. To improve this, we have revised the Results section to include concise summary statements at the conclusion of each major experimental paragraph (Lines 190-191, 201, 218-219, 229-231, 241-242, 272-274, 282-283; 291-293). These additions interpret the data in relation to our main hypothesis. The discussion section was thoroughly revised to more precisely explain the logic supporting the model (Lines 381-393; 433-443, 458-466). Additionally, to bring together the entire dataset, we introduced a new summary schematic (Figure 6A). This figure visually and conceptually integrates our diverse findings, covering metabolic treatments, pH fluctuations, and complex metabolite profiles, showing how these signals work together to control multienzyme complex assembly.

> *This is particularly true for data that seem to reflect more complex trends, such as the GCMS experiments that map metabolites across multiple experiments, or treatments that show somewhat counterintuitive results, such as the antimycin A treatment, which promotes rather than disrupts the MDH1-CIT1 interaction.*

We agree that our complex datasets, including the metabolomics and the seemingly counterintuitive Antimycin A results, required deeper synthesis. To clarify the broader metabolic trends, we have added Figure 6A to visually map which factors, specifically pH, malate, fumarate, and aspartate, most consistently align with complex assembly. We revised the Discussion (Lines 390-393, 439-443) to explicitly conclude that no single variable predominantly governs the interaction, but it is coordinately regulated by multiple microenvironmental cues.

Regarding the Antimycin A (and other ETC inhibitors) discrepancy, where the interaction is enhanced despite suppressed respiration, we have expanded our interpretation (Lines 346–358) to explain this as a transient response that is not directly reflected by steadystate respiratory activity. Specifically, we propose that acute perturbations of the mitochondrial matrix microenvironment, particularly changes in pH, temporarily promote MDH1–CIT1 interaction. Thus, under these conditions, transient microenvironmental changes can dominate over steady-state respiratory output in regulating metabolon assembly.

The discussion paragraph about the imperfect relationship between pH and interaction has been revised to highlight our conclusion that mitochondrial matrix pH can be a contributing factor rather than the primary regulator (Lines 386-393).

> *(2) Some of the assertions put forth in the manuscript are not substantiated by the data presented, and the authors are at times overly reliant on previous findings from the literature to support their claims. This is particularly notable for claims about "TCA cycle flux"; the authors do not perform flux analysis anywhere in their study and should be cautious when insinuating correlations between their observations and "flux".*

We appreciate the reviewer's careful evaluation of our terminology and fully agree that claims regarding "flux" should be reserved for studies that employ direct isotopic flux measurements. In response to this constructive feedback, we have thoroughly reviewed the manuscript to ensure that our assertions are substantiated by the presented experimental data. We have carefully evaluated the use of the term "flux" throughout the Abstract, Introduction, and Discussion, replacing it with more accurate phrases such as "pathway

activity," "respiratory activity," or "mitochondrial respiration" depending on the specific context (Lines 11; 20-21; 50; 111-112; 322-327; 329; 345; 349-350; 442-443; 458466).

We also removed a paragraph discussing the potential role of the MDH1-CIT1 metabolon in the malate-aspartate shuttle (Line 361). We realized the paragraph is highly speculative, and our data do not directly support the hypothesis. The influence of the MDH1-CIT1 on the malate-aspartate shuttle is a major finding of the upcoming manuscript reporting its effects in metabolic network flux. We apologize for mixing up the results of two separate studies.

Furthermore, we have revised our conclusions to avoid over-reliance on prior literature in making causal claims. We now explicitly frame the dynamic assembly of the MDH1-CIT1 metabolon as an integral factor in metabolic regulation, closely related to cellular metabolic states, rather than stating that it controls pathway flux (Lines 454-462). We believe these textual revisions accurately align our claims with our current observations and remove any unsubstantiated assertions.

> *(3) The manuscript presentation could be improved. For figures, at times, the axes do not have intuitive labels (example, Figure 1A), data points and details about the number of samples analyzed are missing (bar graphs and box plots), and molecular weight markers are not reported on western blots. The authors refer to the figures out of order in the text, which makes the manuscript challenging to navigate as a reader.*

We thank the reviewer for these helpful suggestions to improve the clarity and presentation of the manuscript. We have made several revisions accordingly.

First, axis labels have been revised throughout the figures to improve clarity and make them more intuitive. Second, we have added the number of biological replicates to the figure captions and updated bar graphs and box plots to display individual data points. Third, to improve the transparency of the immunoblot data, we have included molecular weight marker position in Figure 1C and corresponding full gel images in a new Figure 1 – figure supplement 2. Other immunoblot images have been moved to Figure 2 – figure supplement 1 since they lack molecular marker images.

In addition, we have reorganized the figure panel labeling and corresponding text to improve the flow of the Results section. Specifically, figure subpanels are now arranged according to the measured parameters rather than treatment conditions, and the relevant sections describing TCA cycle manipulation and ETC inhibition have been revised to follow this updated figure order (Lines 208–231; 251–274). These changes improve the readability and logical progression of the manuscript.

> ***Recommendations for the authors:***
>
> ***Reviewer #1 (Recommendations for the authors):***
>
> *The grammar in the abstract in the sentence which states called metabolon. This needs to be fixed.*

We thank the reviewer for pointing this out. We have revised the sentence in the Abstract to improve clarity. The revised sentence reads: “The tricarboxylic acid (TCA) cycle enzymes malate dehydrogenase (MDH1) and citrate synthase (CIT1) form a multienzyme complex, referred to as a metabolon, that channels intermediate oxaloacetate between their reaction centers.” (Lines 7-9)

> ***Reviewer #3 (Recommendations for the authors):***
>
> *Major points:*

> *(1) Much of the data reported in this manuscript reads as a summary of what was found, rather than distilling what the trends in the data mean or how they support the proposed model.*

We thank the reviewer for this comment. This concern overlaps with your previous point (Weakness 1), which we have addressed through revisions to improve synthesis and clarity. Specifically, we have added concise summary statements at the end of each major experimental section (Lines 190-191, 201, 218-219, 229-231, 241-242, 272-274, 282-283; 291-293), and we have included a new summary schematic (Figure 6A) that integrates the findings to illustrate how metabolic conditions and mitochondrial microenvironments relat to MDH1–CIT1 interaction. Together, these revisions improve the interpretation and clarify how the results support our model.

> *For instance, in Figure 3, the authors use one metabolic treatment to activate the TCA cycle and two to inhibit the TCA cycle. In Figure 3M, GC-MS data are reported for select metabolites across these three conditions, as well as a control condition. However, these metabolites don't follow clean "trends" according to the predictions; as one example, malate is down in the TCA active (acetate) and one TCA inhibited condition (arsenite), whereas it is elevated in the second TCA inhibited (aminooxyacetate) condition. As an additional example, glutamate is down in the arsenite (inhibited) condition, slightly down in the acetate (activated) condition, but is unchanged in the AOA (inhibited) condition. Similar variability is seen in Figure 4M. What do these discrepancies mean? How do they support the model? As written, these data bring forth more questions than they answer.*

We appreciate the reviewer's careful analysis of the metabolomics data in Figures 2E, 3M, and 4M. The reviewer notes that the levels of certain metabolites show complex patterns that do not simply reflect overall TCA cycle activity. We have acknowledged that our metabolomics dataset is a valuable resource for the research community and have added a brief paragraph to emphasize the complex metabolic phenotypes resulting from chemical treatments (Lines 422-431).

As mentioned in the paragraph, this complexity is biologically expected. It is likely from the distinct primary targets of each inhibitor, such as arsenite affecting redox-sensitive enzymes and AOA disrupting the malate-aspartate shuttle, as well as off-target effects and the adaptive reorganization of intersecting metabolic networks to bypass local blockades. Rather than viewing these diverse metabolic phenotypes as discrepancies, we leveraged them to uncouple general respiratory suppression from specific metabolite pools, allowing us to independently assess their relationship with metabolon assembly.

Furthermore, we note that our GC-MS analysis measures whole-cell metabolite levels, which represent the sum of multiple subcellular compartments and may not precisely reflect localized concentrations within the mitochondrial matrix that is directly affected by the TCA cycle. The description of this limitation of whole-cell metabolomics has been revised in Lines 417-420.

> *(2) Why do the authors propose that antimycin A increases the interaction between MDH1 and CIT1 despite decreasing respiratory activity? Given the generalities proposed in Figure 6, this is important to address.*

We thank the reviewer for this comment. This point overlaps with Weakness 1, where we have addressed the apparent discrepancy associated with antimycin A (and other ETC inhibitors). Briefly, we have expanded our interpretation (Lines 349–360) to explain this effect as a transient response that is not directly aligned with steady-state respiratory activity. We propose that acute perturbations of the mitochondrial matrix microenvironment, particularly changes in pH, temporarily promote MDH1–CIT1 interaction. In addition, we

have revised the Discussion (Lines 386–404) to clarify that mitochondrial matrix pH acts as a contributing factor rather than the primary regulator of the interaction. Together, these revisions reconcile the ETC inhibition by antimycin A with the overall model presented in Figure 6.

> *(3) The authors use acetate to "activate" the TCA cycle; do other non-fermentable carbon sources also promote the MDH1-CIT1 interaction?*

We thank the reviewer for this insightful question. We have tested additional nonfermentable carbon sources and found that they did not significantly affect MDH1–CIT1 interaction (Figure 3—figure supplement 1). We note that raffinose present in the medium likely provides a baseline carbon source supporting oxidative metabolism, which may limit the observable effects of these treatments (Lines 149-150).

In addition, we performed a new experiment using ethanol. While ethanol treatment enhanced the MDH1–CIT1 interaction signal, it also increased the abundance of MDH1 and CIT1, resulting in a reduced interaction index. Because ethanol induces protein accumulation under our experimental conditions, this result is not straightforward to interpret. We have included this observation and its interpretation in the revised manuscript (Lines 208–211).

> *(4) The authors show that the MDH1-CIT1 interaction is sensitive to pH. Is the MDH1-CIT1 interaction affected by uncouplers in vivo?*

We thank the reviewer for suggesting a meaningful experiment. We performed a new experiment examining the effect of the uncoupler CCCP on MDH1–CIT1 interaction in vivo (Figure 4—figure supplement 4). We found that CCCP treatment increased the interaction signal, consistent with the idea that acidification of the mitochondrial matrix promotes MDH1–CIT1 association.

However, we observe that CCCP treatment also decreased the luciferase signals from MDH1 and CIT1 fused to full-length NanoLUC in an abnormal way, making it harder to interpret the interaction index. Therefore, although these results support a possible role for pH in regulating the interaction, they should be viewed with caution and included as a figure supplement. This experiment and its interpretation have been added to the revised manuscript (Lines 276–283).

> *(5) NADH is a potent suppressor of many enzymes within the TCA cycle, including MDH1 and CIT1. Can the authors modulate mitochondrial NADH through genetic manipulation of Ndi1, or through overexpression of mito-Lb-NOX (PMID: 27124460)?*

We thank the reviewer for this insightful suggestion. We agree that the mitochondrial NADH is a potential regulator of the MDH1-CIT1 interaction as it is a potent suppressor of many TCA cycle enzymes, and indeed, we have previously shown that NADH inhibit the MDH-CS interaction in vitro (Omini et al 2021 PMID: 34548590). For this reason, we investigated the mitochondrial matrix redox state that is related to the NADH levels in the current study. The reviewer's proposed strategy of using targeted genetic tools like mito-Lb-NOX or Ndi1 manipulation to specifically influence the NADH level is an elegant approach to isolate this variable. However, implementing this system requires generating, optimizing, and validating new yeast strains that harbor the targeted NADH-modulating constructs alongside NanoBiT and full-length NanoLUC sensor systems. Because this extensive strain engineering and subsequent live-cell validation fall outside a feasible timeframe for the current manuscript revision, we must respectfully defer these experiments. We view the precise manipulation of the mitochondrial redox state via tools like mito-Lb-NOX as a complementary approach for our future work to systematically pinpoint the individual regulatory factors. We have expanded our Discussion (Lines 417-420; 462-465) to highlight the targeted genetic manipulation of the possible regulatory factors including the NADH pool, as a critical future direction for dissecting these dynamics.

> *(6) The authors should correct their figures:*
>
> *(a) Axes should be easy to interpret on graphs.*
>
> *(b) Individual datapoints should be shown on bar graphs and box plots. Minimally, the number of samples evaluated should be reported.*
>
> *(c) Molecular weight markers should be reported on blots.*

We thank the reviewer for these helpful suggestions. Points (a) and (b) overlap with Weakness 3, which we have addressed through revisions to improve figure clarity and data presentation. Specifically, axis labels have been revised to be more intuitive, the number of samples is now reported in the figure captions, and bar and box plots have been updated to include individual data points. For time-course data, we retained point-line plots, as alternative formats (e.g., bar or box plots) would reduce clarity due to the density of time points.

For point (c), we have added molecular weight markers to the immunoblot data where available (Figure 1C). In the time-course experiment in the original Figure 2, molecular weight markers were absent from the gel images. Although we are confident in the identity of the detected signals, we have moved these data to a figure supplement (Figure 2—figure supplement 1C) to reflect this limitation. Similarly, the corresponding Co-IP data are now presented as a figure supplement (Figure 2—figure supplement 1A).

> *Minor points:*
>
> *(1) In the last paragraph before the results, the authors refer to "the fluorescent biosensors", but start the paragraph discussing the nanoBIT PPI. After reading the manuscript, these seem to be distinct experimental setups, but that was not evident in the first read through of the paper.*

We thank the reviewer for pointing out this source of confusion. We apologize for the lack of clarity in distinguishing between the experimental approaches. In this study, the NanoBiT system was used to measure MDH1–CIT1 interaction, whereas fluorescent biosensors were used to assess mitochondrial matrix pH, redox state, and ATP levels. We have revised the paragraph to more clearly distinguish these methodologies and their respective roles in the study (Lines 105–112).

> *(2) As mentioned above, referring to multiple figures out of order within the manuscript is very jarring for the reader. The authors should consider reworking the narrative or figures to be presented in order.*

We thank the reviewer for this comment. This concern overlaps with the previous comment regarding figure organization, which we have addressed by revising both the figure labeling and the corresponding text. Specifically, figure subpanels have been reorganized to follow the measured parameters rather than treatment conditions, and the Results sections describing TCA cycle manipulation and ETC inhibition have been revised to follow the updated figure order (Lines 208–231; 251–274). These changes improve the logical flow and readability of the manuscript.

https://doi.org/10.7554/eLife.107953.2.sa0